Biomaterials Science

ROYAL SOCIETY OF CHEMISTRY

REVIEW

View Article Online
View Journal | View Issue

Cite this: *Biomater. Sci.*, 2020, **8**, 5824

Evaluating medical device and material thrombosis under flow: current and emerging technologies

Jun Ki Hong, [a,b,c,d,e] Lingzi Gao, [c,d,e,f] Jasneil Singh, [c,e,g] Tiffany Goh, [c,e,g] Alexander M. Ruhoff, [c,e,f] Chiara Neto [a,d] and Anna Waterhouse *[b,c,d,e,f]

Received 2nd August 2020,
Accepted 30th September 2020

DOI: 10.1039/d0bm01284j

rsc.li/biomaterials-science

Although blood-contacting medical devices are used widely, blood clot formation (thrombosis) leads to device failure and potentially catastrophic adverse thrombotic events for patients, such as stroke or pulomonary embolism. Systemic anti-thrombotic drugs aimed at reducing these complications do not always prevent device thrombosis and can cause increased bleeding risks. Therefore, our understanding of material thrombosis mechanisms needs to be improved in order to develop next generation blood-contacting medical devices and materials. Medical device development requires material thrombogenicity evaluation according to the International Standards 10993-4 *Biological evaluation of medical devices–Selection of tests for interactions with blood*, which highlights that one of the key aspects for testing is a clinically relevant flow system. In this review, we first provide an overview of the current knowledge regarding material thrombosis and important physical and biological aspects of blood flow in relation to thrombus formation. We then examine commonly used *in vitro* flow systems to evaluate material and medical device thrombosis, focusing on their capabilities, advantages and disadvantages. Finally, we explore recent advances in technology that will aid in improving the design and fabrication of flow systems, mechanistic analysis and computational modelling.

1. Introduction

Blood-contacting medical devices are often used to treat a wide range of diseases. Devices range in size, function, material composition, anatomical placement and duration of contact with the blood. Examples of blood-contacting medical devices include stents,[1–3] catheters,[4–6] ventricular assist devices (VADs), artificial heart valves and vascular grafts.[7–9] Despite the many advantages provided by such devices, synthetic biomaterials are affected by biological fouling (biofouling).[10–13] Biofouling of medical devices is the non-specific adsorption of proteins onto material surfaces which then allows cell adhesion. In the presence of microbes this can lead to infection and sepsis,[14,15] and in contact with blood, this can lead to blood clots (thrombosis) and subsequent complications such as occlusive thrombus formation, stroke *via* thrombus embolisation, as well as device failure through 'clogging'.[16,17]

Medical-device induced thrombosis is one of the major complications of implantable medical devices that are exposed to blood.[16,18,19] Virchow's triad describes the 3 key conditions necessary for thrombosis to occur.[20] In relation to material-induced thrombosis, these are the hypercoagulability of the blood (pathology), haemodynamic factors (low flow/stasis or high flow), and medical device materials, shown in Fig. 1A. The typical process by which biomaterial thrombosis occurs is illustrated in Fig. 1B. Due to their high plasma concentrations and high diffusion coefficients, plasma protein adsorption to the material surface is followed by synergistic adhesion and activation of coagulation factors,[21] platelets, leukocytes[11] and/or complement cascade proteins,[21] resulting in thrombosis.[19] A vast number of different types of proteins can adsorb to the surface to initiate thrombosis, including; fibrinogen, high molecular weight kininogen (HMWK), pre-kallikrein (PK), factor XII (FXII), complement proteins, von Willebrand Factor (vWF), and immunoglobulins, leading to complex protein–biomaterial and protein–protein interactions.[22] For example, activation of surface-bound FXII not only triggers thrombin generation *via* the intrinsic pathway of coagulation, but also induces complement activation.[14] In the case of fibrinogen, conformational change after adsorption is the key parameter

[a]*School of Chemistry, The University of Sydney, NSW 2006, Australia*
[b]*School of Medical Sciences, Faculty of Medicine and Health, The University of Sydney, NSW 2006, Australia. E-mail: anna.waterhouse@sydney.edu.au*
[c]*Heart Research Institute, Newtown, NSW 2042, Australia*
[d]*The University of Sydney Nano Institute, The University of Sydney, NSW 2006, Australia*
[e]*The Charles Perkins Centre, The University of Sydney, NSW 2006, Australia*
[f]*Central Clinical School, Faculty of Medicine and Health, The University of Sydney, NSW 2006, Australia*
[g]*School of Biomedical Engineering, Faculty of Engineering, The University of Sydney, NSW 2006, Australia*

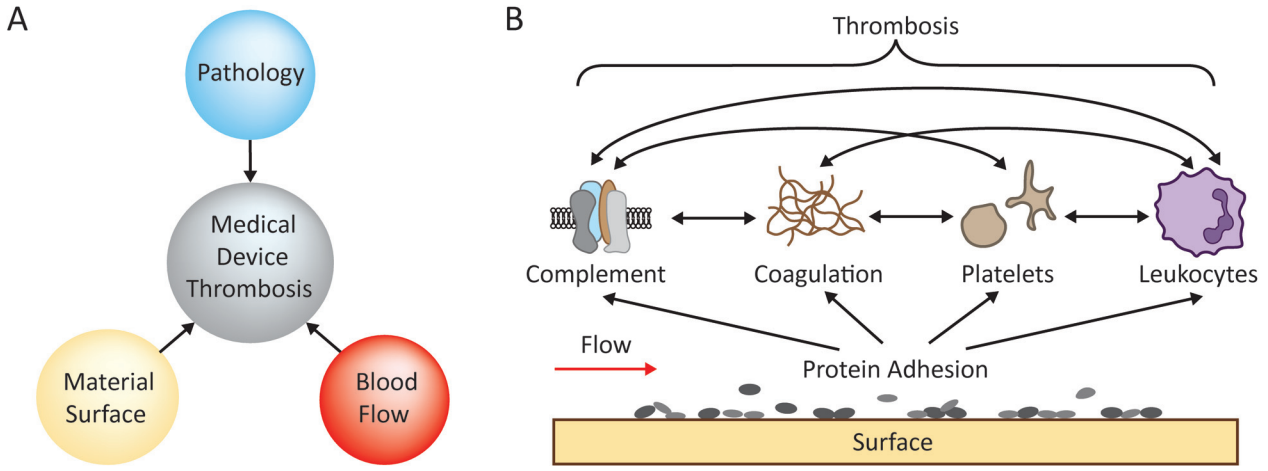

Fig. 1 (A) Modified Virchow's Triad for factors contributing medical device thrombosis including; exposure to a foreign material surface, pathology or state of hypercoagulability and the presence of blood flow, or lack thereof. (B) Illustration of plasma protein and adsorption and activation of blood components from each potentially contributing pathway and the interplay of those pathways that lead to thrombosis on the surface of medical device materials.

for platelet adhesion and activation rather than adsorbed quantity.[23] On the surface of materials, the adsorbed amount and conformation of these plasma proteins is dependent on material surface properties such as wettability,[24] surface charge,[25] chemistry, and topography.[26–28] The adsorbed protein layer subsequently dictates the activation of coagulation, platelets, and leukocytes. For a detailed review of the thrombogenicity of biomaterials, we direct readers to a recently published review series.[10–12,14] Variations in medical device type, implant location and geometry can induce disturbed flow conditions (both low and high flow, see section 2), making the interplay of biological pathways complex. Ultimately, our understanding of the mechanisms which underpin material-induced thrombosis is still incomplete.[14,29,30]

Current clinical solutions to medical-device thrombosis involves the administration of anticoagulants such as heparin, warfarin and/or antiplatelet therapies.[17] However, they have the continued risk of bleeding complications and do not

Jun Ki Hong

Jun Ki Hong graduated with a BSc (Hons I) from the University of Sydney in 2017 with a double major in Chemistry and Cell Pathology. He is currently carrying out his PhD on understanding the biofouling of materials used in blood-contacting medical devices under the supervision of Prof. Chiara Neto and Dr Anna Waterhouse. Jun also has commercial industry experience, having spent time between the start-up environment and the corporate world in a key stakeholder management role, working to commercialise technologies such as biosensors and energy storage devices.

Chiara Neto

Professor Chiara Neto is an Australian Research Council Future Fellow in the School of Chemistry at the University of Sydney. She is internationally recognised for her work on interfacial slip, thin liquid films and functional nanostructured and patterned surfaces. She has conducted her career across several countries: she received her Masters and PhD degrees at the University of Florence, Italy. Then she did research at the University of Ulm and at Saarland University on the dewetting of thin polymer films (2002–2003). In 2003 she moved to the Australian National University (Canberra) when she was awarded an Australian Research Council fellowship to work on nanorheology. Since 2007 she has established at the University of Sydney the Nano-Interfaces group, which focuses on investigating the wetting and flow properties of liquids at nano- and micro-structured surfaces. Prof. Neto is one of the Founding Directors and former President of the Australasian Colloids and Interface Society.

always prevent medical-device thrombosis.[14] Despite the development of many new medical devices, materials and surface coatings in recent decades, we have generally failed to decrease medical device thrombosis clinically or reduce the need for anti-thrombotic therapies.[7,22,31–33] As such, there remains an unmet clinical need for low and anti-thrombogenic materials for blood-contacting medical devices.[19,31,34]

There are a number of reasons for the lack of understanding of blood–material interactions,[35] one in particular is due to a lack of standardised, predictive *in vitro* and *in vivo* haemocompatibility tests.[35–38] The International Standard Medical Device Testing – ISO 10993-4 (*Biological evaluation of medical devices – Selection of tests for interactions with blood*) describes the recommended methods of testing for medical devices that interact with blood for regulatory purposes.[3,30,38,39] According to these Standards, the characterisation of blood interactions with medical devices and materials should mimic the clinical conditions as closely as possible and analysis should be performed to assess activation of the major pathways and key factors involved in medical device thrombosis (depending on the device type): thrombosis, coagulation, platelets, haematology, and complement.[40] Given these criteria, and that the majority of blood-contacting medical devices used clinically are exposed to flowing blood, the ISO10993-4 suggests model systems should include clinically relevant blood flow conditions and use whole blood.[41,42] A number of different *in vivo* and *in vitro* models and systems have been developed for this purpose, each with specific advantages and disadvantages.[29,43] *In vivo* animal models allow evaluation of medical devices or materials with whole blood under physiological flow conditions; however, they can be cost prohibitive and time consuming.[40] More importantly, animal model data may not be an accurate representation of clinical device performance due to the considerable variations in blood composition, anatomy and physiology between species.[44,45]

In vitro blood flow models for testing the thrombogenicity of device materials typically use human whole blood or separated blood components from volunteer donations, and are generally less costly.[36] Small sample volumes allow for replicate testing of multiple materials and controls simultaneously using the same batch of blood. In combination with controlled flow conditions, temperature and anticoagulation, *in vitro* methods can provide further insights into thrombotic processes that may occur on medical device materials.[36] Nonetheless, they are not without their own set of limitations. The lack of activation-inhibiting functions of endothelial cells and blood recirculation in model systems can result in accumulation of activated cells and proteins and cause the material-induced thrombotic reactions to occur more quickly which prevents studies longer than a few hours being carried out with *in vitro* methods.[36,40] As such, a combination of methods are required to effectively assess the potential translation of materials to clinical applications. Utilising and further developing *in vitro* systems to their fullest potential will aid in the development of future anti-thrombogenic medical devices and materials.

1.1 Overview

This review highlights and summarises some of the commonly used *in vitro* methods for analysing blood–biomaterial interactions dynamically. The focus is particularly on methods that include the effect of blood flow, which has a key role in governing thrombus formation (see section 2). We first describe the flow and biological parameters relevant to medical device thrombosis. Second, we describe some common systems used to evaluate and study material haemocompatibility, highlighting their applications, distinct advantages, as well as their limitations. We conclude by providing an outlook into the development of new techniques to assess and understand the dynamic interplay of events at the blood–material interface. Such strategies include the utilisation of cutting-edge bioengineering tools and advances in microscopy techniques as well as computational fluid dynamic modelling.

Understanding the complex interactions of medical device materials with blood, proteins, and cells is essential for the development of more sophisticated materials for the next generation of blood-contacting medical devices such as those used in the treatment of cardiovascular disease. Some proposed materials in development include the immobilisation of anti-thrombogenic or thrombolytic proteins and biomolecules or the fabrication of anti-fouling coatings.[11,12,46] However, this is beyond the scope of the current review and instead, we direct interested readers to numerous recent reviews on novel anti-thrombogenic and thrombolytic surface coatings and materials.[47–53]

2. Blood flow-induced medical device thrombosis

Blood flow in the body is driven by the physiological action of the heart or is imparted by the mechanical movement of the

Anna Waterhouse

Dr Anna Waterhouse leads the Cardiovascular Medical Devices Group in the School of Medical Sciences, Faculty of Medicine and Health at the University of Sydney and is an affiliated Group Leader at the Heart Research Institute. She received her PhD from the University of Sydney and conducted her post-doctoral research at the Wyss Institute for Biologically Inspired Engineering at Harvard University. In 2016, she received a Discovery Early Career Researcher Award from the Australian Research Council and established her multidisciplinary research group, which focuses on biological interactions at material interfaces combined with cardiovascular medical device engineering, specializing in material thrombosis and bioinspired approaches to improve and design new medical devices and diagnostics.

medical device. The interplay between blood flow and thrombus formation is complex and several reviews have summarised important flow features of blood.[54,55] In order to describe blood flow in vessels and constrained geometries typical of medical devices, it is useful to define first, in simple terms, a few concepts used in fluid dynamics.

2.1 Physical basis of blood flow and fluid dynamic properties

2.1.1 Shear rate and viscosity. Flow within blood vessels is pressure-driven, and is often approximated with Poiseuille flow, such as the one depicted in Fig. 2A, where a fluid is flowing within a pipe of diameter D. As shown in the schematic, the velocity (v) of the liquid has a gradient within the pipe, being highest in the centre of the pipe and decreasing to zero according to a parabolic function near the stationary wall.[56,57] The velocity gradient near the wall is called wall shear rate ($\gamma = dv/dz$, units of s^{-1}). The fluid velocity is slowed down by the inherent resistance to flow within the fluid (quantified by the viscosity of the fluid) and by the friction between the fluid and the stationary walls of the pipe. Two measures of viscosity are often used: the dynamic viscosity (η, SI unit is N S m^{-2} or Pa s) and kinematic viscosity ($\mu = \eta/\rho$, where ρ is the density of the fluid; SI unit is $m^2\ s^{-1}$, but the c.g.s. unit Stokes, St, is still used).

2.1.2 Wall shear stress. Wall shear stress (τ, SI units Pa, but the c.g.s. units are still used, 1 dyne per cm^2 = 0.1 Pa) is the tangential force (along the direction of flow x in Fig. 2A) per unit area that is exerted by the flowing fluid on the surface (wall) of the pipe. Its magnitude is equal to:

$$\tau = \eta\gamma = \eta\frac{dv}{dz}. \quad (1)$$

Wall shear stress τ increases with increasing velocity gradient near the vessel wall and increasing fluid viscosity. It is important to quantify wall shear stress in blood vessels because the flow interacts with the vessels endothelium.[58] For example, in arteries at regions with lower wall shear stress, blood components have longer residence times near the wall, and this has been associated with higher risk of atherosclerosis.[59]

2.1.3 Laminar flow and turbulent flow. Laminar flow is the regime in which the streamlines of liquid flow parallel to each other and parallel to the vessel wall; flow within regions of the vasculature where blood flow is slow and blood vessels have a small diameter is laminar.[59] Flow is defined as laminar when the Reynolds number, R_e, is much smaller than 1; the Reynolds number is:

$$R_e = \frac{\rho}{\eta}vr \quad (2)$$

where r is the radius of the capillary, η is the viscosity and ρ the density of the fluid. On the other hand, for flow through larger vessels, and in medical devices where v may be high, the Reynolds number for pipe flow can become large and the flow regime then changes. For $R_e > 2300$ the flow starts to transition and for $R_e > 4000$, pipe flow becomes turbulent, which means that complex flow patterns, such as eddies and vortices, can develop.[60,61]

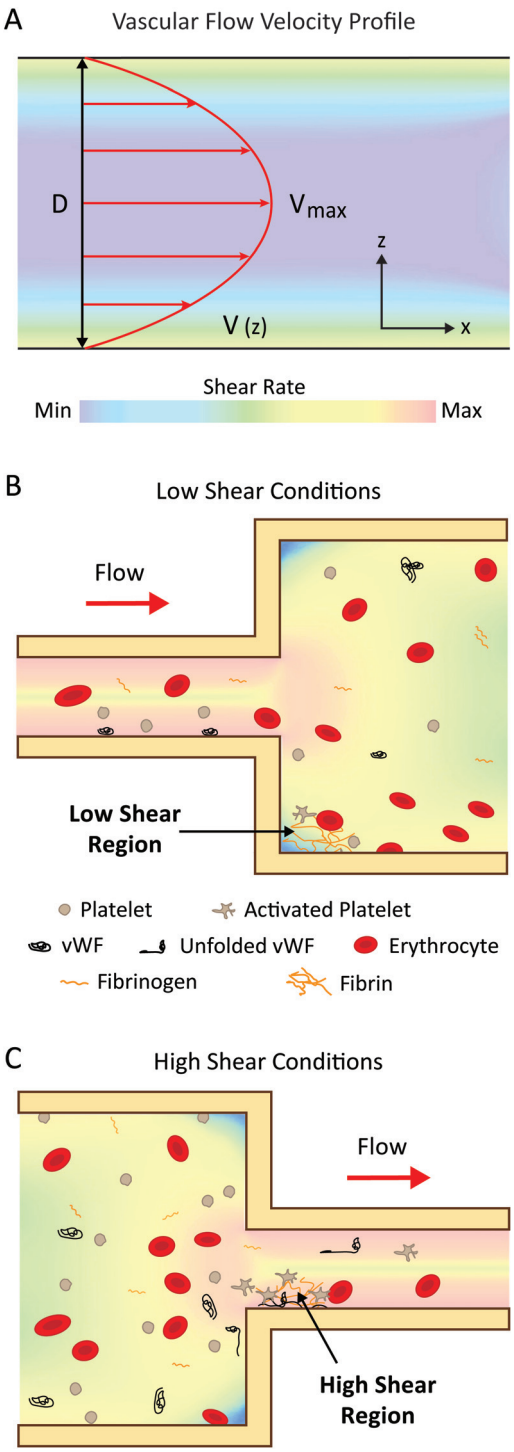

Fig. 2 (A) Schematic of flow of blood within a blood vessel can be approximated by Poiseuille flow with maximum flow velocity in the centre of the vessel and minimum at the wall where the opposite is true for shear rate. (B) Blood flow under low shear conditions. (C) Blood flow under high shear. The colour scale bar in (A) applies to parts (A), (B) and (C), and the legend in (B) applies to (C).

2.1.4 Newtonian liquids. Liquids are defined as Newtonian when their behaviour is ideal *i.e.* when their behaviour under shear can be described by eqn (1) and their viscosity decreases monotonically for increasing temperature but does not depend on the shear rate or of time of observation. Examples of Newtonian liquids are water ($\eta^{20°C}$ = 1.002 mPa s), olive oil (η = 99 mPa s) and glycerol (η = 2330 mPa s). Other fluids, including blood, which contains complex components such red blood cells (erythrocytes), white blood cells (leukocytes) and proteins behave differently depending on the time scale of the application of stress and the time of observation. Whole blood is a non-Newtonian liquid, and its viscosity changes non-monotonically with the applied shear stress,[62,63] attributed mainly to erythrocyte behaviour. Under low shear, erythrocytes aggregate in stacks (rouleaux) increasing blood viscosity (shear-thickening) and under high shear conditions, these aggregates dissociate and erythrocytes can deform to alight with the direction of flow, resulting in lower viscosity (shear-thinning).[64] Therefore, whole blood flow is often approximated with that of a Newtonian liquid at high shear rates.[58,59] Blood plasma on the other hand, behaves as a Newtonian fluid with a constant shear viscosity.[65,66]

2.2 Implications of blood flow for medical device thrombosis

Physiologically, shear stress in blood vessels of differing sizes usually ranges between 2 and 36 dyne per cm^2 (Table 1). There are well-established associations between fluid dynamic parameters such as stagnation, high shear stress and turbulence, and thrombotic processes such as coagulation and platelet activation and aggregation.[20,67] Low blood flow increases transport and diffusion of proteins and cells to surfaces, increasing the residence time of prothrombotic components on a surface and causing leukocyte adhesion.[20,21] Additionally, high shear rate and stress induced by blood flow can affect mechanosensitive proteins and cells and cause thrombus formation.[29,68] These are discussed further in sections 2.3.1 and 2.3.2.

The shear forces in medical devices are typically far greater than those found in the body as shown in Table 1 (40–20 000 dyne per cm^2). Considerable variation in shear stress can occur within the one device, such as catheters and ventricular assist devices, which introduce both low and high shear stress conditions depending on their size, placement and geometric configuration.[69,70] Of note, the highest shear rate in peripherally inserted catheters is caused by the mixing of the infusion solution with the blood at the catheter tip/endothelium/blood interface.[69] Turbulent blood flow can occur in medical devices at regions of expansion, bifurcations, and joints/connections.[71] Variations in device design can also affect haemodynamics, for example, the different pump mechanisms in left ventricular assist devices (axial and centrifugal flow pumps), have differing blood residence times and shear rates.[72,73] Additionally, it is worth noting that shear and turbulence can increase drastically during exercise, for example, in coronary stents.[74]

2.3 Haemodynamic implications for thrombus formation

In the following sections, we will elaborate on the biological mechanisms affected by variations in flow described in section 2.2. For the purposes of this review, we will classify shear rates as 'low' and 'high'. 'Low' shear rates refer to a range between 0–1000 s^{-1}, which are shear rates generally found in the veins, most arteries, and many medical devices. 'High' shear rates refer to values greater than 1000 s^{-1}, which occur in specific arteries, pathological conditions, (such as atherosclerosis), and also found in number of medical devices (Table 1).

2.3.1 Low shear rate regime. Stasis or low shear can promote accumulation of coagulation factors, leukocytes, and erythrocytes. Coagulation initiation on a surface is regulated by the biochemical reactions of the coagulation pathway and blood flow.[21] Under low shear conditions (<1000 s^{-1}), coagulation factors diffuse to the surface and accumulate. Once a threshold concentration is reached, biochemical reactions

Table 1 Typical blood flow properties of blood-contacting medical devices and human anatomy

	Flow rate (mL min^{-1})	Wall shear stress (dyne per cm^2)	Maximum shear strain rate (s^{-1})	Ref.
Anatomical locations				
Aortic valve	5000	4–11	20	94–98
Large arteries	250–500	14–36	300–800	83, 99 and 100
Coronary artery	120–300	5–15	800–2500	101–103
Stenotic vessels	120–180	36–450	800–10 000	83, 99 and 103
Large veins	200–700	2–3.4	10–500	84, 104–106
Medical devices				
LVAD pump	5400	6000	171 429[a]	99 and 107
ECMO pump	4000	1750	50 000[a]	108
Peripheral intravenous catheter 2.1 mm	28 (blood flow rate) 240 (infusion rate)	20 000	571 429[a]	69 and 109
Peripheral intravenous catheter 1.1 mm	28 (blood flow rate) 60 (infusion rate)	1000	28 571[a]	69 and 109
Coronary stent	120	40	11 000	74, 103 and 110–113
Prosthetic heart valve	5000	2400	68 571	114–119

Left ventricular assist device (LVAD); extracorporeal membrane oxygenator (ECMO). [a] Calculated from eqn (1), assuming dynamic viscosity of human whole blood to be 3.5 mPa s at 37 °C.[120] Medical device values are maximum with references representing ranges from different device types. Catheter dimensions are outer diameter.

dominate thrombus formation and the enzymatic coagulation cascade becomes activated, converting fibrinogen into fibrin resulting in a fibrin-rich thrombus, traditionally associated with venous thrombosis.[75,76] Further details of the transport mechanisms governing these phenomena, mathematical models and experimental validation were recently reviewed by Rana and Neeves.[20]

As well as coagulation factor accumulation, cell adhesion can occur at low shear rates. Leukocyte adhesion is initiated above a shear stress threshold of ~0.5 dyne per cm^2 and rolling occurs optimally between ~0.5–1.5 dyne per cm^2. This process is regulated by the mechanical behaviour of specific classes of adhesion receptors on the leukocytes and endothelial cells on blood vessel walls.[77] Additionally, erythrocytes, originally thought to only play a passive role in thrombosis, are now appreciated to be actively involved. At low shear rates, erythrocyte rouleaux increases blood viscosity and leads to increased local concentrations of coagulation factors.[20] Furthermore, there is increasing evidence for the role of erythrocyte adhesion to the vessel wall and adhesion to growing thrombi, both indirectly and directly *via* fibrin and von Willebrand Factor (vWF).[78]

Although platelets can bind to fibrinogen at low shear (100–300 s^{-1})[79] they are not activated at low shear rates and therefore are not thought to contribute significantly to thrombosis under low blood flow conditions.

In relation to medical devices, changes in device geometry such as expansions and connections can cause regions of low flow, recirculation and stagnation (Fig. 2B). These regions have a higher propensity for coagulation and subsequent thrombotic complications, observed from computational modelling and clinical data,[69,80,81] such as in catheters, extracorporeal device connection points, and haemodialysis access sites.[29] The introduction of catheters to veins can impede blood flow and cause occlusion of the vessel, leading to regions of low velocity and recirculation.[69] These effects are increased with larger sized catheters with flow rates being reduced by up to 93% in some cases.[80] Indeed, clinical meta-studies of peripherally-inserted central catheters revealed an increased risk of venous thromboembolism with the use of larger-diameter catheters[81] and a decreased risk with the use of smaller-diameter catheters.[82]

2.3.2 High shear rate regime. Platelets, vWF and erythrocytes are mechanically sensitive to high shear stress (Fig. 2C).[68,83] In areas of high shear stress (>1000 s^{-1}) such as those in arteries, thrombi are platelet rich.[84] It is now well-established that platelet adhesion, activation and aggregation occurs specifically under high shear stress conditions and shear gradients, in the absence of soluble agonists.[84,85] Physiologically, platelets adhere to exposed collagen and vWF on injured endothelium, with platelets preferentially binding to vWF at high shear rates.[84,86] Under high shear rates, vWF undergoes conformational changes and elongates to expose the A1 domain which allows binding of the platelet glycoprotein receptor Ib (GPIb).[87,88] For a surface-immobilised vWF, the crucial shear rate to induce conformational change was estimated to be around 3000 s^{-1} in platelet-rich plasma (PRP) and ~1000 s^{-1} for whole blood.[87] The shear-induced conformational changes also cause polymerisation and self-association of vWF at high shear rates of >10 000 s^{-1} which greatly enhances vWF-platelet binding.[84]

In addition to the shear-induced activation of platelets and vWF, erythrocytes are also sensitive to high shear stress and turbulence, which can cause membrane rupture and release of haemoglobin.[17,89] Subsequent free haemoglobin can cause a number of thrombotic complications such as hypercoagulation,[90,91] thromboembolism,[78] and platelet activation induced by a reduction in nitric oxide bioavailability.[78,91–93]

These mechanosensitive properties of blood have major consequences for the thrombogenicity of medical devices. For instance, stents implanted in coronary arteries are exposed to high shear stress which causes platelet activation, requiring patients to receive dual anti-platelet therapies to prevent stent thrombosis.[121,122] In VADs, the extremely high shear stress induces vWF conformational changes which exposes degradation sites for the protease ADAMTS-13, resulting in rapid depletion of large vWF multimers, leading to poor vWF-platelet adhesion and a bleeding condition known as acquired von Willebrand Syndrome.[99] Furthermore, haemolysis and associated complications can be caused by artificial heart valves,[123] haemodialysis circuits,[124] and VADs.[16]

3. Methods to assess thrombosis on medical device materials under flow

In this section, we will highlight some of the most common *in vitro* analysis methods which incorporate flow that are used to assess the interaction of biomaterials with blood and blood components, summarised in Table 2. We briefly describe the operating principle of each method along with some examples of their utility and application for studying the thrombogenicity of various materials under blood flow. Given its importance in designing and interpreting experimental model systems, we will first give a brief overview of computational fluid dynamic (CFD) simulation of blood flow in relation to medical devices and *in vitro* model systems.

3.1 Computational fluid dynamic modelling of blood flow in medical devices and *in vitro* models

As medical device thrombus formation is material[16] and flow dependent,[67] numerical characterisation of the haemodynamic conditions within medical devices, including, but not limited to velocity, pressure and wall shear stress, is critical. The flow changes due to blood-contacting medical devices such as catheters (Fig. 3A),[69] stents,[110,111] and mechanical valves (Fig. 3B)[115,125] have been widely modelled using CFD simulations, as have *ex vivo* devices and tubing systems.[126] CFD simulations of more geometrically complex medical devices such as ECMO[108] and LVADs (Fig. 3C)[107,127] require more advanced, specialised knowledge and are more computation-

Table 2 Summary of common methods used for assessing medical device material thrombogenicity under blood flow *in vitro*

Method	Shear strain rate (s^{-1})	Advantages	Disadvantages	Ref.
Chandler loops	50–428	• Whole blood • Simple • Low cost • Material inside tubing or tubing itself	• Narrow shear range • Only mimics low shear medical devices • Recirculation • End-point assay • Medium blood volume (~3–20 mL per sample)	134, 146, 152 and 153
Flow loops	50–82 143	• Whole blood • Medically relevant pumps/devices can be incorporated or material inside tubing or tubing itself • Time point sampling possible • Single pass flow possible	• Medical device flow/shear difficult to replicate unless medical device is used to drive flow • Recirculation (generally) • Large blood volume (~50–100 mL per sample) • Haemolysis (unless evaluating haemolysis)	134, 144 and 152
TEG/ROTEM	0.1–0.5	• Whole blood or plasma • Low blood volume (<1 mL per sample) • No effects of stasis (Virchow's Triad) • Fast results and real-time outputs	• Only low shear • Non-physiological flow pattern • Baseline variability across individuals • Choice of material limited to cup material or coating thereof	154–161
Cone-and-plate rheometry	0.1–10 000	• Whole blood or platelets • Wide range of shear rates • Easily interchangeable sample material • Physical clot properties at known time-point • Low blood volume (<1 mL per sample) • Potential for real-time measurements	• Complicated flow regimes at higher shear rates • Cone material is usually not modifiable • Possibility of fluid evaporation over time	158 and 162
Parallel plates and microfluidic devices	50–1000	• Whole blood or platelets • Wide range of shear rates • Low blood volume (<1 mL per sample) • Real-time measurements • Desired geometry possible to replicate wide range of flow conditions • Materials/coatings can be incorporated	• Replicating turbulence is difficult at the microscale • Impact of viscosity effects is greater	148, 163–170

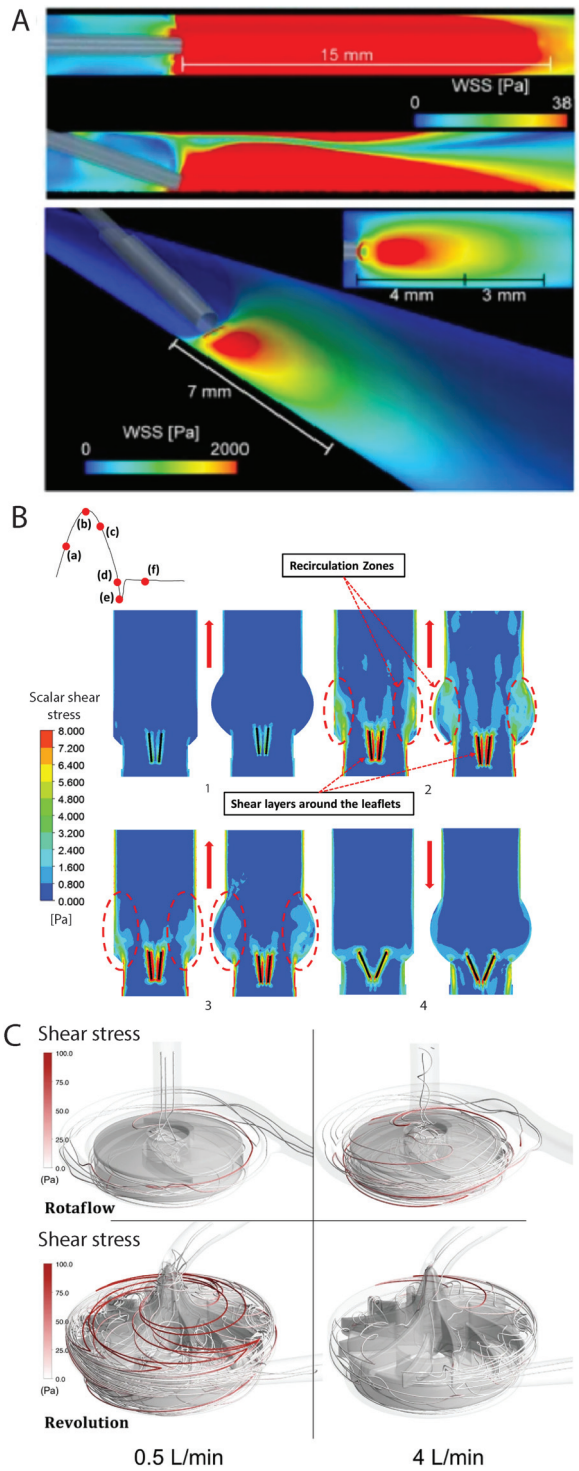

Fig. 3 Computational fluid dynamic (CFD) modelling is commonly used to model medical devices. (A) Wall shear stress (WSS) of catheter placement in a blood vessel.[69] Reproduced from ref. 69 with permission from Springer Nature, copyright 2018. (B) CFD model showing high shear stress, stagnation and recirculation near the leaflets of a bileaflet mechanical heart valve (at 0 degree tilt) in straight or anatomic aortas, during different phases of the cardiac cycle (1–4).[125] Reproduced from ref. 125 with permission from John Wiley and Sons, copyright 2020. (C) Shear stress on a particle streamline of a centrifugal pump used in extracorporeal oxygenation machines (ECMO).[108] Reproduced from ref. 108 with permission from Springer Nature, copyright 2019.

ally expensive to accurately model. However, this is particularly important due to the widely varying geometries of components such as centrifugal pumps, roller pumps, and oxygenators. These contain dramatic expansion and contraction of flow at inlets, outlets, and in pump regions, which lead to turbulent flow, fluctuating viscosity, fluctuating velocity, and zones of stagnation.[128] For example, previous CFD models from multiple groups have identified the shear stress range in LVAD impellors to range between 0–6000 dyne per cm^2,[99,107,129,130] however from the simulations it can be noted that 99% of the blood volume does not experience shear stress greater than 500 dyne per cm^2 (Table 1). However, this is similar for most devices. Additionally, dedicated simulations can be conducted that specifically investigate thrombus formation, for example, the positioning of an LVAD outflow cannula in the aorta significantly affect thrombus distribution throughout the aorta due to the altered aortic flow conditions.[131] CFD models of *in vitro* experimental systems are useful for rigorous design of the model, to characterise the model set up and flow conditions, and to interpret results.[132] They are referred to in subsequent parts of section 3.

3.2 Test flow loops

Flow loops vary widely in their design and method of imparting fluid flow.[29,30] Flow loops allow the evaluation of thrombus formation directly *via* thrombus weight, as well as surface thrombosis using microscopy such as scanning electron microscopy (SEM).[133] In blood sampled from these loops, cell number and activation state, and protein levels and activation state, can be measured *via* flow cytometry, enzyme-linked immunosorbent assays respectively, and desired specific assays can be carried out, for example, for haemolysis.[133,134]

Importantly, blood flow measurements allow comparison of results to clinical or medical device flow parameters. Laser Doppler and laser speckle are useful techniques for measuring flow rates in vessels *in vivo*,[135–137] however, these generally provide relative flow measurements and laser speckle is limited by its poor depth specificity.[138] Therefore, they are not generally used for investigating biomaterial thrombogenicity, although laser speckle or laser Doppler have been used to compare or calibrate flow rates in tubing or capillary tubes *in vitro*, prior to *in vivo* use.[139–141] In contrast, Doppler ultrasound provides quantitative flow rate measurements and has been used to measure blood flow in *in vivo* models of device thrombogenicity, for example, vascular grafts,[142] as well as to measure blood flow in *in vitro* models of circuits containing medical devices[143] or tubing systems.[136,137,144]

The simplest flow loop system is the modified Chandler loop which uses a rotating wheel to drive blood flow in tubing loops and is an established method for investigations into material thrombosis under flow.[145] Materials can either be placed inside or used as the tubing (Fig. 4A), allowing blood contact under flow rates of 25–200 mL min^{-1}, replicating venous and coronary artery flow rates (Table 1). Modified Chandler loops have been used to measure a variety of materials, with specific tests driven by the aims of each investi-

gation (Table 2). For example, to investigate the haemocompatibility of alternative materials for prosthetic heart valves, Brubert *et al.* placed various block co-polymers in a modified Chandler loop, exposing materials to blood flow at shear rates up to 300 s^{-1}. Platelet and coagulation cascade activation on these materials was reduced relative to polystyrene and while more thrombogenic than clinically used alternatives including bovine pericardium, inflammation was reduced.[146]

A key advantage of modified Chandler loops is the ability to incorporate whole blood into a simple, relatively low-cost setup to study material thrombogenicity under flow. However, these loops have several limitations. They require a large blood volume to test multiple materials and controls and the assays are usually end point. Modified Chandler loops are closed systems which recirculate the same, small blood volume over the material surface, which can overestimate the thrombogenicity of materials due to accumulation of activated blood components. While suitable for replicating low shear strain rates, to our knowledge, modified Chandler loops have not replicated shear rates above 500 s^{-1} (Table 2). Additionally, the paucity of CFD simulations of modified Chandler loops has impaired our understanding of flow conditions within these systems, with some studies indicating that, due to the tubing curvature, traditional straight tube approximations of flow are inaccurate at higher rotation rates.[147]

To overcome the flow limitations of Chandler loops for testing medical grade tubing, components and devices, large flow loops powered by peristaltic pumps,[133,134,148] and flow loops linked directly to medical device circuits (*e.g.* LVAD,[133,149] ECMO[148]) have been used (Fig. 4B and C). The peristaltic pump flow loop pumps blood from a reservoir, through a tubing loop and back to the reservoir (Fig. 4B). The peristaltic pump generates pulsatile flow more characteristically similar to that observed *in vivo*, as flow velocity and thus the resulting rheological conditions may be controlled by varying the pump power and frequency.[127,134] Furthermore, these pumps are used in clinical haemodialysis and cardiopulmonary bypass circuits. Previously van Oeveren *et al.* mimicked coronary blood circulation in peristaltic flow loops using a flow rate of 40 mL min^{-1} to generate a shear stress of 12 dyne per cm^2.[134] Similar to the modified Chandler loop, the material being tested may be placed inside or used as the tubing of the loop. Meanwhile for medical device flow loops, a loop is formed by tubing connected between the inlet and outlet of the medical device, in which part of the tube contains a fill port and outlet port from which the circulating blood is filled and removed (Fig. 4C). As the medical device being tested is part of the loop, flow and shear rate conditions such as those of the LVAD and ECMO are more easily replicated, and the material surface being tested is contained within the medical device component.[133,148,149]

Key advantages of large flow loops compared to modified Chandler loops include the ability to achieve and control a wider range of flow and shear rate conditions and to recirculate larger volumes of blood, allowing evaluation of actual clinical devices. However, they require acquisition of large volumes of fresh blood and haemolysis can occur due to blood recirculation (although this is not a disadvantage if evaluating rates of haemolysis).[134] Furthermore, generating CFD models of peristaltic flow to ascertain the precise flow and shear conditions within the large flow loop experimental setup is much more difficult than producing CFD models for fully-developed, 'smooth' flow experimental systems.[127,150,151] Previous attempts to computationally model peristaltic pump systems revealed that flow and shear conditions are significantly affected by the wall geometry (highlighting the gap between CFD assumptions and experimental models).[127]

Arising from the need for a flow loop system which produces higher shear rate ranges while minimising haemolysis, the Haemobile ball valve model was recently designed to generate flow waves most similar to that of *in vivo* physiological conditions, compared to modified Chandler loops and large flow loops.[134] The pulsatile flow within the loop is controlled by a ball valve in the cylindrical chamber of the flow loop, which also ensures uni-directional flow of blood within the loop.[144] A Doppler ultrasound flow probe was used to determine flow rates and subsequently calculate the wall shear stress and confirm pulsatile flow patterns.[144] The only drawback is that it is still a closed loop system. So far, the Haemobile has been used successfully to evaluate the thrombogenicity of polymer tubing and vascular graft materials.[134,144]

3.3 Thromboelastrography (TEG)/rotational thromboelastometry (ROTEM)

TEG/ROTEM are viscoelastic methods of monitoring clot formation. These tests consist of a plastic cup and a pin attached to a torsion wire (Fig. 4D and E). In TEG, the cup oscillates 4.75° every 5 seconds (Fig. 4D), while in ROTEM the pin oscillates 5.25° every 6 seconds, inducing low shear rates analogous to venous blood flow (Fig. 4E).[161] In response to recalcification, fibrin fibre formation increases torsion on the wire, which is detected as clot firmness.[156] These assays provide several useful indicators of material thrombogenicity, including: time to fibrin formation or clotting time, rate of clot formation, maximum clot strength and clot susceptibility to fibrinolysis.[156,161] Shear stress in TEG/ROTEM is low (0.1–0.5 dyne per cm^2) however, limited CFD information is available for how these numbers were derived.[155,157] TEG/ROTEM systems are predominantly used clinically to diagnose a range of coagulopathies including trauma induced coagulopathy and to assess bleeding risks during cardiac surgery.[161]

TEG/ROTEM is an easy and effective technique which shows promise for assessing the effects of low shear on biomaterial coagulation. Recently, TEG has been utilised to study the thrombogenicity of material surface coatings applied to the base cup under low flow. The anti-adhesive, omniphobic tethered-liquid perfluorocarbon (TLP) surface coating applied to TEG cups displayed increased clotting time, reduced rate of clot formation and reduced clot strength relative to untreated Cryolite® (acrylic polymer) cups. Furthermore, TLP displayed faster fibrinolysis compared to control cups.[160] Similarly, a

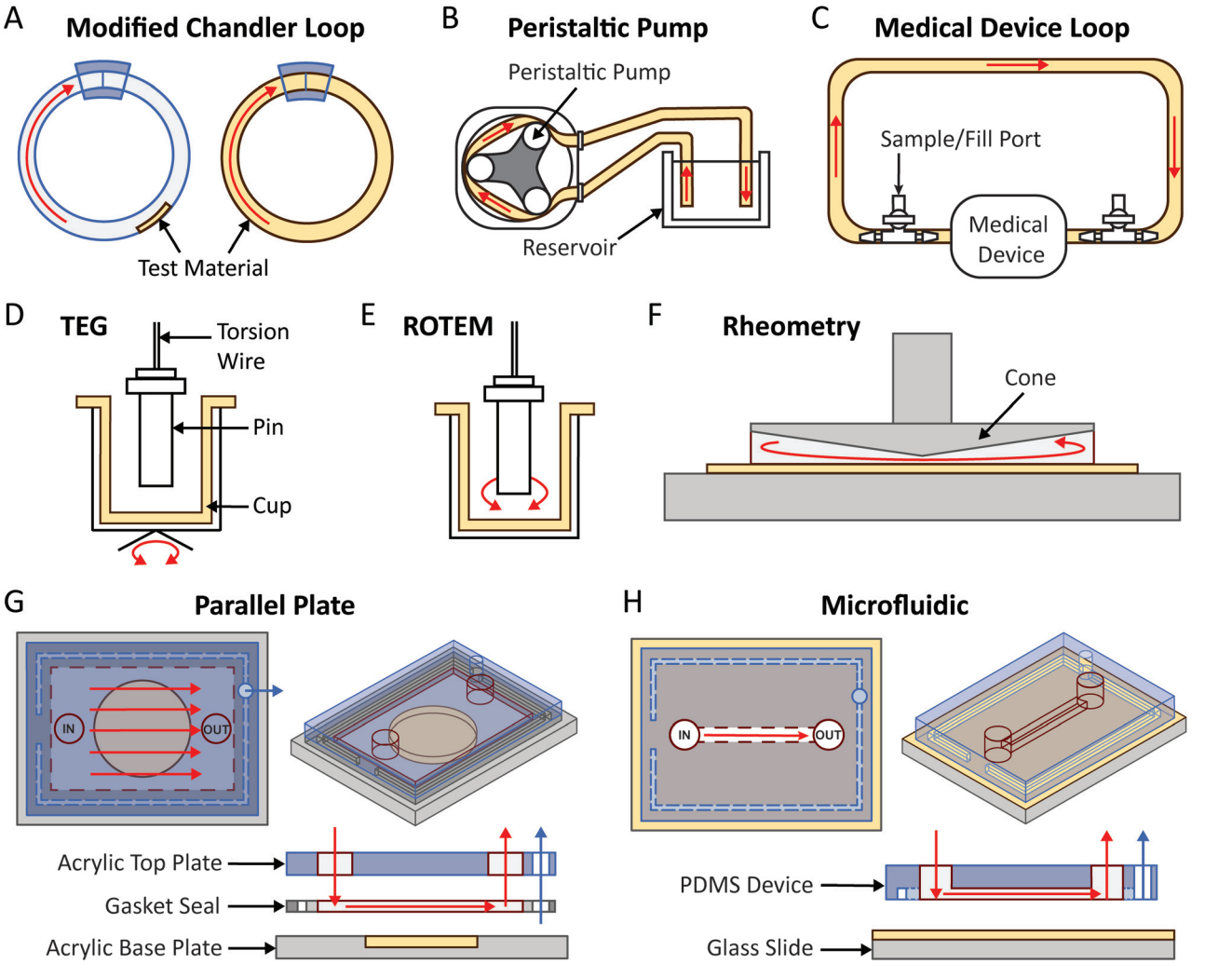

Fig. 4 Illustrations of commonly used methods to assess the thrombogenicity of materials under blood flow. (A) Modified Chandler loops showing the test material can be placed inside the tubing loop or is the tubing loop. (B) Large flow models. (C) Medical device loop. (D) Thromboelastography (TEG). (E) Rotational thrombogelastometry (ROTEM). (F) Cone-and-plate rheometer. (G) Parallel plate. (H) Microfluidic devices. Test materials are colour coded in beige while the direction of blood flow is indicated by red arrows. Blue arrows in (G) and (H) refer to applied vacuum.

poly(carbonate-urea)urethane polymer coating incorporating polyhedral oligomeric silsesquioxanes displayed reduced maximum clot strength and increased clot lysis at 60 minutes post-thrombus formation.[154,171]

TEG/ROTEM have several limitations. TEG/ROTEM recycles the same volume of blood throughout the assay in a non-physiological flow pattern. Furthermore, the cup material is currently limited to polymethylmethyacrylate (PMMA, acrylic) in ROTEM and Cryolite® in TEG.[161] Thus, material thrombosis studies are currently restricted to surface modifications which can be applied to the cups supplied with the TEG/ROTEM analysers. In TEG®6s and ROTEM® Sigma devices, the test cup comes integrated into microfluidic channels which contain reservoirs with lyophilised activator or inhibitor reagents (*e.g.* tissue factor).[122,123] While this modification has allowed even faster thrombogenicity/haemostasis monitoring clinically, utilisation of older models to study biomaterial thrombosis might be most appropriate due to detachable cups allowing facile material modifications (*e.g.* with surface coatings). Finally, it is worth noting that there is high variability between individual blood donors necessitating the use of baseline measurements if comparison to clinical data is desired.[172]

3.4 Cone-and-plate rheometry

Cone-and-plate (CP) rheometry has been used for decades to study haemorheology and blood coagulation processes.[63,173,174] The cone-and-plate set-up typically consists of a rotating cone on top of a flat baseplate, with the fluid of interest between the conical surface and the baseplate as illustrated in Fig. 4F. The angular separation between the cone surface and the base-plate usually varies between 0.5°–5°,[175] which allows it to maintain uniform shear stress on the fluid of interest (independent of the radial location and the gap clearance).[176,177] The rotation of the cone can be varied to

impart different shear rates while the cone geometry can confer varying shear stresses as well as producing turbulent flow at high shear rates.[176,178] Some applications of the CP rheometer in the context of blood rheology and coagulation have included measurement of platelet activation,[83] blood viscosity,[65] erythrocyte aggregation, haemolysis,[64,179] effect of shear stress on whole blood coagulation,[158,159] and thrombus contraction.[180,181]

To assure that the desired fluid shear stress and shear rate are reflected in the experimental setup, CFD simulations have been used to model cone and plate apparatuses. Important parameters influencing thrombus formation that should be considered in CFD modelling include the cone surface and base-plate angle, the rotation and the heat transfer occurring between the cone and fluid.[182] The accuracy of cone and plate CFD models is limited by the temperature and diffusion profile of the cone to disk gap, assumptions for the Nusselt and Sherwood numbers for heat transfer,[182] whether a non-slip (zero velocity) assumption applies at fluid-surface boundary,[183] whether flow may be assumed to be unidirectional,[184] and accurately modelling the non-Newtonian properties of blood.

The cone-and-plate rheometer has also found applications in the testing of materials thrombogenicity and propensity for protein and cellular adsorption to artificial surfaces.[185–187] These studies include the interaction between platelets and erythrocytes on synthetic surfaces such as stainless steel, PMMA and PEO-modified PMMA where the number of platelets in an aggregate were dependent on the material and shear rate (more platelets per aggregate for hydrophilic surfaces and at higher shear rates).[188] Conversely, increased shear rates led to the decrease in the number of platelet-erythrocyte aggregates.[188] Another study of platelet adhesion to tetrafluoroethylene-propylene copolymer surfaces suggested that shear-induced platelet ADP release determines the deposition, following the activation of thrombin.[189,190] Interestingly, this is not the case for artery subendothelium.[191] Recently, the study of platelet aggregation on carbon-based ceramic coatings under blood flow revealed interesting insights into the different mechanisms of aggregate formation.[192] Platelet aggregation on hydrophobic carbon-coated surfaces at shear rates of 1800 s^{-1} was found to be dependent upon platelet activation. Under the same shear conditions, platelet aggregation on the more hydrophilic carbon-coatings were not shown to be reliant on the platelet activation state.[192]

Some of the advantages provided by the cone-and-plate method includes the ability to impart uniform shear stress across the sample and over a wide range of shear conditions (up to order of 10^5 s^{-1}),[162] and the ability to test different materials, with relatively small blood volumes with the potential for real-time outputs.[174,177] A similar set-up with parallel plate geometries exists, (not to be confused with parallel plate flow chambers as discussed in section 3.5) which utilises a flat, rotating plate instead of a cone geometry. However, the parallel plate geometry imparts non-uniform shear stress due to the varying radial velocity of the flat plate.[193]

The limitations of the cone-and-plate system are that the technique does not reproduce the exact conditions of the blood flow such as in the case where eddy currents and regions of disturbed flow arise upon cellular adsorption causing undulations in the topography of the sample surface.[64,176] Importantly, the testing of modified materials is limited to the sample placed on the baseplate since the cone is left unmodified which may influence the adhesion of blood components, depending on the cone material.[194] Additionally, the rheological data are influenced heavily by the utilised geometries and are susceptible to user errors caused by incorrect blood sample loading such as underfilling or overfilling and the inclusion of trapped air and air bubbles.[64,195–197]

3.5 Parallel plate & microfluidics

Parallel plate and microfluidic flow devices are miniaturised flow models which have been used extensively in the field of haematology ranging from early straight channel glass capillary flow chambers to more recent custom devices.[86,148,198] Studies using these devices have included the impact of surface adsorbed coagulation proteins on platelet adhesion,[199] shear strain rates on vWF elongation,[200] and shear gradient dependent platelet activation.[67] The same techniques have been explored for clinical use in diagnostic applications.[201,202]

There are no strict criteria differentiating parallel plate and microfluidic flow systems, and in some cases these terms are used interchangeably.[203–205] Broadly, parallel plate flow chambers have channel cross sections with smaller height to width ratios and simpler flow paths (Fig. 4G and H). Velocity distribution through the channel cross section changes depending on the height to width ratios of the channel, from square (1.0) to parallel plate (0.0).[206] Theoretical shear stress profiles for commonly used rectangular channels of finite width are highest at channel faces and drops to zero at the corners.[207] Shear stress profiles in devices with complex geometries can be characterised with CFD to ensure the desired flow characteristics are replicated *in vitro*.[148]

Miniature flow models with channel geometries closer to parallel plate flow are commonly constructed by sandwiching a gasket (which defines the height) between two plates on which the surface of interest is mounted (Fig. 4G). A vacuum can be applied through the gasket to seal the flow channel and prevent device separation. In comparison, microfluidic devices can vary widely in channel complexity to generate complex flow paths. Devices can be formed using a variety of fabrication methods, most commonly by casting channels in elastomeric polymers, *e.g.* polydimethylsiloxane (PDMS) (Fig. 4H), termed soft lithography, from moulds fabricated utilising photolithography techniques. This result in channels with an open rectangular cross section, which are sealed by adhesion to a base containing the material of interest, to create an enclosed device (Fig. 4H). For both systems, precise flow control can be achieved using syringe or peristaltic pumps.

These systems have been applied to the study of thrombosis on medically relevant materials through the incorporation of a broad range of relevant polymers, metals and coatings in par-

allel plate and microfluidic devices. For example, platelet adhesion to various polymers and metals was investigated under flow, without[165–169,208] or with pre-adsorption from protein solutions or plasma[163,209] at shear strain rates of 43–1000 s^{-1}. Notably, Jamiolkowski *et al.* measured dynamic adsorption of platelets over time to a range of medically relevant opaque materials using a suspension of platelets and cleared erythrocytes to minimise light scattering enabling surface visualisation by epifluorescence microscopy. The medical grade titanium alloy, Ti6Al4V, supported high levels of platelet adhesion, which was more pronounced at the highest shear strain rate (1000 s^{-1}), compared to silicon carbide, alumina, coated titanium alloy (MPC-Ti6Al4V), yittria partially stabilised zirconia, and zirconia toughened alumina.[165] Unique flow effects such as stagnation caused by crevice geometries,[164] or due to sudden expansion of a flow path can also be modelled at this scale.[166] Kragh *et al.* showed decreased platelet embolisation on carbothane compared to pelethane, with increasing embolic events at lower flow rates (<100 s^{-1} compared to ~500 s^{-1}), using a stagnation point flow chamber, where whole blood flow originated from a single point and spread radially across the surface.[166] Additionally, the thrombogenicity of surface coatings has been evaluated using parallel plates or microfluidics. A tetraglyme coating reduced platelet adhesion compared to control, observed by real-time microscopy,[210] and pressure measurements in a microfluidic channel showed a prolonged thrombus formation time on the anti-adhesive, TLP coating compared to control.[211]

Advantages of parallel plate and microfluidic devices include the replication of key aspects of fluid flow *in vitro* such as wall shear stress, shear strain rates, and fluidic effects resulting from channel geometry.[148] Due to their small scale and low perfusion volumes these models allow the conservation of donor blood and reagents while maintaining physiologically relevant single pass flow where blood or individual blood components are passed over a test surface without recirculation. Dynamic changes in surface platelet adhesion and thrombotic events can be monitored through microscopy revealing aspects of thrombosis not seen on end-point or fixed samples.[164–166,208] This technology has become more accessible over time as many commercial miniature flow systems have become available.

There are, however, limitations to these models as miniaturisation can also be a weakness. Flow at this scale is laminar, therefore, it is not possible to induce turbulent flow unless the smallest channel dimension is greater than 500 μm.[148] Additionally, aspects of microscale blood flow should be considered when designing microfluidic models. Flow in small vessels (<1 mm) and therefore microfluidic channels, is non-Newtonian, meaning, the cell free layer at the vessel wall occupies a larger portion of the vessel, which decreases the viscosity of the blood, known as the Fahraeus-Lindqvist Effect.[212,213] Channel dimensions also influence shear stress distribution in rectangular cross sections, therefore, lower height to width ratios should be used when even shear stress distributions are desired across the width of the channel.[214,215]

3.6 Remarks on current blood flow-material evaluation methods

A wide variety of flow systems are utilised to evaluate medical device thrombogenicity under flow, each providing numerous and varied data outputs. Here we described the advantages and disadvantages of the most commonly used techniques including peristaltic pump driven flow systems, modified Chandler loops, TEG/ROTEM, cone and plate rheometry, parallel plates and microfluidics. Flow loops and Chandler loops require larger volumes of blood but can measure multiple soluble markers from the blood. They can also evaluate medical devices directly, making them useful for translational studies. TEG/ROTEM allow evaluation of clotting parameters that are comparable to clinical measurements using low blood volumes, however, they can only operate under low flow conditions. Shear-induced adhesion and activation of blood proteins and cells has been made possible with cone-and-plate rheometry, and parallel plate or microfluidic systems. These systems require lower volumes of blood and can operate under a wider range of shear stress conditions. Furthermore, the parallel plates and microfluidic systems can provide real-time outputs such as pressure and microscopic visualisation, and are single pass flow systems compared to the flow loops and cone-and-plate rheometers which continuously expose materials to the same blood sample over the duration of the experiment.

Medical device thrombosis is a complex, multi-phase process involving protein/cellular adhesion, clot growth and thrombolysis. Therefore, a single method cannot provide accurate assessment of all aspects of material thrombosis. It is clear that a combination of different methods should be employed in order to thoroughly evaluate the thrombogenicity of materials for applications in medical devices. Naturally, this could include the development of new and improved methods (both experimental and computational) that can offer an enhanced understanding of the processes underlying materials thrombosis. The following section (section 4) will explore some emerging bioengineering and characterisation techniques that could be employed for future investigations that aim to study the dynamic interaction of blood and materials. Of note, the examination of material thrombogencitiy should always be closely aligned to those outlined in the ISO 10993-4 standards and will also require effective pre-clinical, animal models in order to complement the understanding of the safety and efficacy of blood-contacting materials for potential future applications.

4. Emerging bioengineering and characterisation techniques

Recent progress in microfabrication, microscopy, and other multidisciplinary fields have enabled greater understanding of numerous physiological and pathological processes. Application of these novel techniques and adaptation of older

techniques to the field of biomaterial thrombosis presents an opportunity to advance testing systems, knowledge and ultimately improve medical devices. We will highlight some exciting advances that could be used to develop model systems to address specific gaps in the field, improve analysis methods to obtain greater insight into dynamic events in material thrombosis, and advances in computational modelling that could improve accuracy of models and better predict outcomes of newly developed anti-thrombotic materials.

4.1 Microfabrication for advanced experimental system design

Fabrication techniques on the milli- to nanometre scale have improved dramatically in recent decades. This has enabled more complex geometries to be incorporated into flow systems that replicate physiological and pathological conditions.[148] Traditional soft lithography limits these channel shapes to rectangular structures and thus, they do not mimic the geometries of medical devices. Mannino *et al.* produced cylindrical channels using thin optical fibres as moulds (Fig. 5A). Changes in the optical fibre shape created complex channel geometries, with these used to develop vascular models of aneurysms, bifurcations, and stenoses (Fig. 5B).[216] This low-cost and simple fabrication process could be adopted to replicate specific desired geometries of medical devices on a small scale.

Stereolithography (SLA), a more advanced additive manufacturing technique, has enabled the reproducible fabrication of microfluidics with complex geometries, cross-sectional channel resolution down to 18 μm × 20 μm (ref. 217) and low surface roughness.[218] Using SLA, Costa *et al.* 3D-printed microfluidic replicas of healthy and stenotic blood vessels from patient computerised tomography scans (Fig. 5C–H).[219] The ability to combine patient- and device-specific geometries with rapid prototyping techniques could allow personalised evaluation of medical device complications.

Another emerging fabrication technique is Two-Photon Polymerisation (2PP) lithography.[220] This enables fabrication of fluidic systems with complex 3D architectures and nanoscale resolution. By combining standard photolithography with 2PP, channel widths of 420 nm have been fabricated in a non-cleanroom environment.[220] However, the high cost and long print times have so far restricted use to specialised applications requiring significant precision.[221] Recent attempts at customising the printing setup have significantly reduced print times.[220,222] With a wider adoption of such systems, further advances in medical device mimetic models will be likely.

In addition to developing model systems with more sophisticated geometries, incorporation of more medically relevant materials could improve model systems. Traditionally, microfluidic systems are fabricated from glass and PDMS. However, glass is not generally used in medical devices and silicone is only used in a subset of medical devices. Recently, microfluidics have been fabricated out of a wide range of medically relevant polymers including polyurethane,[223] polycarbonate, polyvinylchloride, and polytetrafluoroethylene,[224] although the specific properties of these materials used for research differ from their clinically used counterparts, partly due to differences in the manufacturing and finishing processes.[224] Furthermore, with advances in blood-contacting tissue engineered constructs for medical applications such as vascular grafts[225] and heart valves,[226] these tissue engineered materials could also be incorporated into experimental systems to evalu-

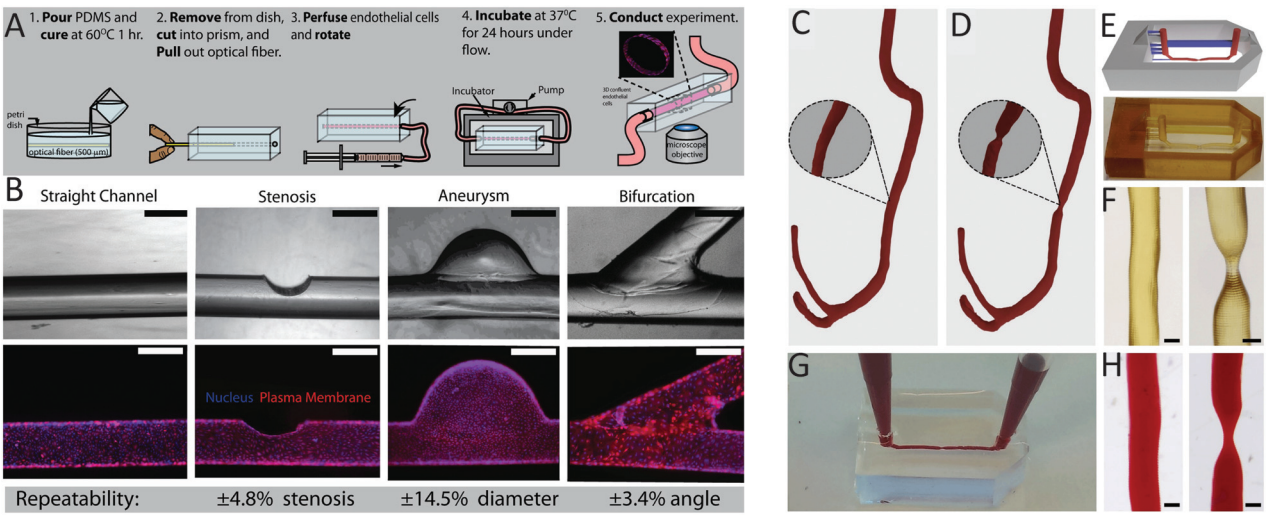

Fig. 5 Novel fabrication techniques for microfluidic models. (A) Casting PDMS around optical fibres generated perfusable models of (B) straight vessels, stenoses, aneurysms and bifurcations.[216] Complex, patient-specific geometries were obtained from computed tomography scans, modelling (C) healthy and (D) stenotic vessels. (E) Higher resolution 3D-printing technologies including stereolithography were used to develop microfluidic moulds of those geometries. (F) Geometric features were accurately reproduced with high resolution. (G and H) Microchannels were perfusable, enabling experiments with whole blood.[219] (A and B) Reproduced from ref. 216 with permission from Springer Nature, copyright 2015. (C–H) Reproduced from ref. 219 with permission from the Royal Society of Chemistry, copyright 2017.

ate their thrombogenicity.[227,228] It should be noted that many of these techniques are for use to generate micron scale flow channels and if studies on turbulence are desired, larger channel dimensions are necessary as discussed in section 3.5.

4.2 Microscopic analysis for medical device thrombosis

Recent microscopy advances which overcome the technical limitations of conventional microscopes present the opportunity to capture material thrombosis events under flow with improved spatiotemporal resolution. Super resolution microscopy (SRM) techniques have recently pushed the boundaries of resolution to the tens of nanometre scale and offer the opportunity to study material–protein and material–cell interactions in greater detail to understand the cellular and molecular mechanisms involved in material thrombosis. The optimal choice of the SRM method depends on the *in vitro* experimental set-up. Generally, structured illumination microscopy (SIM) is better suited for live 3D-imaging due to reduced light intensity allowing longer imaging with less phototoxicity. For example, SIM has recently been used to observe dynamic cell rolling in a microfluidic flow model.[229,230] However, the reduced light intensity comes at the expense of spatiotemporal resolution relative to other SRM methods.[231]

To capture highly dynamic material thrombosis events in flowing blood, it is important to be able to acquire volumetric data at high speed with sufficient axial resolution. Suitable methods include, spinning disk confocal microscopy and lattice light sheet microscopy (LLSM). For example, LLSM was recently utilised to image leukocyte interactions with the vascular endothelium under flow in 3D, in an *in vivo* zebrafish model.[232] New advances combining LLSM with adaptive optics (AO-LLSM) has helped to enhance spatial resolution.[233] Of note, AO-LLSM was used to image the *in vivo* interactions of human breast cancer cells with zebrafish vascular endothelial cells.[233] To our knowledge, LLSM is yet to be applied to *in vitro* biomaterial thrombosis flow models. The requirement for open working space above the sample and immersion into media for imaging in LLSM means spinning disk confocal microscopy is currently better suited for imaging enclosed *in vitro* blood flow experiments.

Live imaging deep within whole blood biomaterial thrombi is limited currently due to increased light scattering with increased tissue penetration, particularly due to the large number of opaque erythrocytes in whole blood. Combining two-photon imaging or spinning disk confocal microscopy with tissue clearing has enabling imaging up to a millimetre into fixed and cleared whole blood thrombi.[234] This technique enables assessment of differences in thrombus formation at the biomaterial surface and in bulk solution. However, drawbacks include the necessity for end point analysis, long tissue processing time, and possible sample shrinkage.[234]

In addition to advances in microscopy techniques themselves, integrating microscopy with traditional flow techniques can provide more detailed information. For example, placing an inverted microscope under the baseplate of a custom cone-and-plate rheometer has previously been employed to observe the differential responses of cells under shear stress.[179,235–237] This method could potentially allow the simultaneous acquisition of rheological information, as well as real-time visualisation of changes to the thrombotic behaviour of blood on various materials under applied shear. The main drawback of this method to study the thrombogenicity of materials is that the materials need to be optically transparent to allow for the acquisition of microscopy data, however, this is also the case for many of the microscopy techniques discussed here.

Finally, developments in approaches to data analysis is another area which could further complement and enhance the capability of microscopy techniques. Image processing techniques utilising machine learning have been used recently to rapidly classify platelet morphology in large data sets.[238] Similar techniques could potentially be employed to monitor platelet response to material surfaces, for instance. This type of automation saves time and reduces human error and bias.

4.3 Computational modelling for medical device thrombosis

As previously discussed, CFD modelling is a valuable tool in the study of haemodynamic flow conditions *in vivo*, *in vitro*, and *in situ*. However, remaining challenges are associated with replicating aspects of flow dynamics, device material properties, and incorporating biological pathways when modelling medical devices and experimental systems.

Flow dynamics in medical devices and *in vitro* often involve pulsatile, low shear and turbulent regimes. As previously discussed, (section 2) blood behaves as a non-Newtonian fluid under low shear conditions.[62,65] Studies comparing different approaches to modelling both pulsatile[150,151,239] and non-Newtonian blood flow,[240,241] revealed variability in the results of fluid flow parameter numerical maps. Therefore, to improve accuracy of models in these flow regimes, further studies could validate computational models with experimental data using methods such as particle tracking velocimetry (PTV),[242] and laser Doppler velocimetry (LDV).[97] These techniques are valuable to determine blood flow patterns in models of medical devices (Fig. 6),[97,243,244] however, their use to correlate

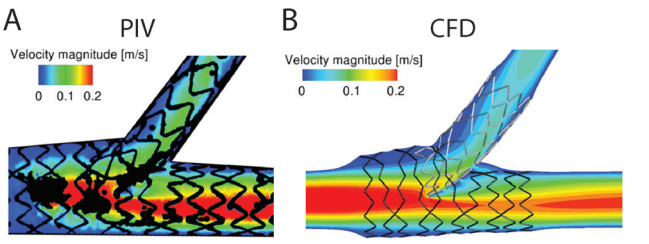

Fig. 6 (A) Particle image velocimetry (PIV) and (B) computational fluid dynamic (CFD) comparisons of the fluid velocity profiles modelled in stented artery.[243] For devices where fluid dynamic conditions may be difficult to computationally model, PIV may be used to gain experimental data. Alternatively, experimental PIV models may be used to verify CFD models. Figure reproduced from ref. 243 with permission from SAGE Publishing, copyright 2015.

flow parameters with material thrombogenicity in experimental *in vitro* flow systems is lacking. With advances in microscopy discussed in section 4.2, future improvements in this area are possible. For example, spinning-disc confocal microscopy allowed velocity profiles to be generated at desired depths throughout the microfluidic channel using an RBC suspension (20% haematocrit),[245] and high-speed confocal microscopy revealed temperature-dependent changes in blood cell dispersion (using 12% haematocrit).[246] Furthermore, turbulence can be a challenge to model and study experimentally,[71,247] and the accuracy of the CFD turbulence models are limited by the accuracy of the chosen computational equations. Micro particle image velocimetry (microPIV),[248–251] LDV[249–251] and 3D PTV[252] have been useful tools to study turbulence. However, the accuracy of microPIV, LDV and PTV are limited by data acquisition speed, because microturbulence is challenging to capture and track.[249]

In addition to flow, the accurate modelling of material surface properties in a CFD model is important as material surface properties significantly influence protein adhesion and subsequent thrombus formation.[10,11] The exact surface properties which result in such phenomena (*e.g.* wettability,[24] surface charge,[25] chemistry and topography[26–28]) are not easily converted into parameters for use in CFD models. For example, surface roughness, is often introduced into CFD simulations by altering the surface friction coefficient.[253,254] While useful for characterising the bulk fluid dynamics at surfaces, this approach does not account for the complex protein and cellular interactions with the surface material, which contribute to material thrombosis.

Mathematically modelling biological pathways has also been applied to the field of thrombosis to predict overall thrombus growth,[255] coagulation,[20] platelet activation,[256] and platelet adhesion and aggregation.[257,258] A future direction for assessing thrombosis *in vitro* and in medical devices is through CFD modelling combined with mathematical models of the biomechanical and biochemical pathways involved in thrombus formation. Ultimately, all mathematical and computational models need to be supported by experimental validation and improved *in vitro* experimental flow systems to understand material interactions with biological systems.

5. Conclusions

Methods to test the performance of blood-contacting medical devices should account for the multitude of factors which reflect their end-use and carefully weigh up their benefits against the potential risks. Such factors for consideration include materials, medical device design and the clinical conditions under which the medical devices are handled, implemented, and operate. Haemodynamics is a key parameter of medical device thrombosis due to its crucial role in governing thrombus formation as well as the potential for the devices to be exposed to disturbed blood flow (or the lack thereof), during clinical applications, and should be appropriately reflected in the testing of material and device thrombosis.

This review explored the advantages and disadvantages of the range of available *in vitro* methods that are commonly used to assess the interaction of medical devices and materials with blood under flow conditions. While many models exist, there is no single method which allows accurate assessment of all aspects of material thrombosis. Multiple methods should be used to evaluate the thrombogenicity of materials, surface coatings, or medical devices, in alignment with ISO 10993-4 Standards. Furthermore, while traditional material development and medical device evaluation has used blood flow loop systems such as the modified Chandler loop and peristaltic pump driven flow, a more mechanistic understanding of material thrombosis is possible with cone-and-plate rheometry, and parallel plate or microfluidic systems, because these systems require lower volumes of blood, can operate under a wider range of shear stress conditions and can provide real-time outputs.

As the field reaches maturity, we can hope to see studies that are able to include higher levels of complexity to more closely mimic relevant clinical scenarios. Improvements in engineering systems, design and production capabilities have enabled researchers to fabricate more advanced testing models on smaller scales with geometries to replicate clinically relevant flow conditions, increased resolution, and to incorporate device-specific materials. Continuing progress in other closely aligned areas of research such as high speed and high-resolution microscopy and computational fluid dynamics modelling can be utilised for biomaterial thrombosis studies to gain more in-depth knowledge of material thrombogenicity. Improved methods for assessing biological interactions with materials under blood flow, and for evaluating their potential for clinical applications will enable the development of safer blood-contacting medical devices.

Abbreviations

μ	Kinematic viscosity (SI unit: $m^2\ s^{-1}$) (c.g.s unit: Stokes, St)
γ	Wall shear rate (SI unit: s^{-1})
η	Dynamic viscosity (SI Unit: Pa s)
2PP	Two-photon polymerisation
CFD	Computational fluid dynamics
CP	Cone and plate (in the context of cone and plate rheometry)
D	Diameter
ECMO	Extracorporeal membrane oxygenation
FXII	Factor XII
GPIIb	Platelet glycoprotein receptor Ib
HMWK	High-molecular weight kininogen
ISO	International organisation for standardisation
LDV	Laser Doppler velocimetry
LLSM	Lattice light-sheet microscopy
AO-LLSM	Adaptive optics lattice light-sheet microscopy

PDMS	Polydimethylsiloxane
PMMA	Polymethylmethacrylate
PK	Pre-Kallikrein
PRP	Platelet-rich plasma
PTV	Particle tracking velocimetry
PIV	Particle image velocimetry
R_e	Reynolds number
ROTEM	Rotational thromboelastometry
SEM	Scanning electron microscopy
SIM	Structured illumination microscopy
SLA	Stereolithography
SRM	Super-resolution microscopy
TEG	Thromboelastography
TLP	Tethered-liquid perfluorocarbon
ν	Velocity (SI unit: m s^{-1})
VAD/ LVAD	Ventricular assist device/left ventricular assist device
vWF	Von Willebrand factor
τ	Wall shear stress (SI unit: Pa)(c.g.s. unit: dyne per cm^2, conversion 1 dyne per cm^2 = 0.1 Pa)

Conflicts of interest

There are no conflicts to declare.

Acknowledgements

JKH acknowledges the Australian Government Research Training Program (RTP) Scholarship, The University of Sydney RTP Supplementary Scholarship and The Heart Research Institute for support. CN acknowledges funding from the Australian Research Council (ARC) under the Future Fellowship scheme. JS and TG acknowledge support from the School of Biomedical Engineering, University of Sydney. AW acknowledges funding from the ARC DECRA (DE160101308), The University of Sydney, Heart Research Institute, The University of Sydney Nano Institute, Clive and Vera Ramaciotti Foundations Health Investment Grant and Vanguard Grant (103004) from the National Heart Foundation of Australia.

References

1 J. Aoki, A. J. Lansky, R. Mehran, J. Moses, M. E. Bertrand, B. T. McLaurin, D. A. Cox, A. M. Lincoff, E. M. Ohman, H. D. White, H. Parise, M. B. Leon and G. W. Stone, *Circulation*, 2009, **119**, 687–698.
2 A. B. Lumsden, M. G. Davies and E. K. Peden, *J. Endovasc. Ther.*, 2009, **16**, II31–II62.
3 F. Jung, C. Wischke and A. Lendlein, *MRS Bull.*, 2011, **35**, 607–613.
4 J. Hou, J. Zhang, M. Ma, Z. Gong, B. Xu and Z. Shi, *Thromb. Res.*, 2019, **184**, 38–43.
5 L. J. Walshe, S. F. Malak, J. Eagan and K. A. Sepkowitz, *J. Clin. Oncol.*, 2002, **20**, 3276–3281.
6 W. Geerts, *Hematology Am. Soc. Hematol. Educ. Prog.*, 2014, **2014**, 306–311.
7 G. D. Dangas, J. I. Weitz, G. Giustino, R. Makkar and R. Mehran, *J. Am. Coll. Cardiol.*, 2016, **68**, 2670–2689.
8 S. P. Pinney, A. C. Anyanwu, A. Lala, J. J. Teuteberg, N. Uriel and M. R. Mehra, *J. Am. Coll. Cardiol.*, 2017, **69**, 2845–2861.
9 M. R. Mehra, *Eur. Heart J.*, 2019, **40**, 673–677.
10 J. L. Brash, T. A. Horbett, R. A. Latour and P. Tengvall, *Acta Biomater.*, 2019, **94**, 11–24.
11 M. Gorbet, C. Sperling, M. F. Maitz, C. A. Siedlecki, C. Werner and M. V. Sefton, *Acta Biomater.*, 2019, **94**, 25–32.
12 M. F. Maitz, M. C. L. Martins, N. Grabow, C. Matschegewski, N. Huang, E. L. Chaikof, M. A. Barbosa, C. Werner and C. Sperling, *Acta Biomater.*, 2019, **94**, 33–43.
13 Y. Wo, E. J. Brisbois, R. H. Bartlett and M. E. Meyerhoff, *Biomater. Sci.*, 2016, **4**, 1161–1183.
14 I. H. Jaffer and J. I. Weitz, *Acta Biomater.*, 2019, **94**, 2–10.
15 L. Liu, H. Shi, H. Yu, S. Yan and S. Luan, *Biomater. Sci.*, 2020, **8**, 4095–4108.
16 T. Hilal, J. Mudd and T. G. DeLoughery, *Res. Pract. Thromb. Haemostasis*, 2019, **3**, 589–598.
17 I. H. Jaffer, J. C. Fredenburgh, J. Hirsh and J. I. Weitz, *J. Thromb. Haemostasis*, 2015, **13**(Suppl 1), S72–S81.
18 A. V. Finn, M. Joner, G. Nakazawa, F. Kolodgie, J. Newell, M. C. John, H. K. Gold and R. Virmani, *Circulation*, 2007, **115**, 2435–2441.
19 P. K. Qi, M. F. Maitz and N. Huang, *Surf. Coat. Technol.*, 2013, **233**, 80–90.
20 K. Rana and K. B. Neeves, *Blood Rev.*, 2016, **30**, 357–368.
21 M. B. Gorbet and M. V. Sefton, *Biomaterials*, 2004, **25**, 5681–5703.
22 C. A. Labarrere, A. E. Dabiri and G. S. Kassab, *Front. Bioeng. Biotechnol.*, 2020, **8**, 123.
23 B. Sivaraman and R. A. Latour, *Biomaterials*, 2010, **31**, 832–839.
24 H. T. Spijker, R. Graaff, P. W. Boonstra, H. J. Busscher and W. van Oeveren, *Biomaterials*, 2003, **24**, 4717–4727.
25 C. Sperling, M. Fischer, M. F. Maitz and C. Werner, *Biomaterials*, 2009, **30**, 4447–4456.
26 L. Zhang, B. Casey, D. K. Galanakis, C. Marmorat, S. Skoog, K. Vorvolakos, M. Simon and M. H. Rafailovich, *Acta Biomater.*, 2017, **54**, 164–174.
27 A. Toscano and M. M. Santore, *Langmuir*, 2006, **22**, 2588–2597.
28 C. Blaszykowski, S. Sheikh and M. Thompson, *Biomater. Sci.*, 2015, **3**, 1335–1370.
29 S. Sukavaneshvar, *Adv. Drug Delivery Rev.*, 2017, **112**, 24–34.
30 S. Braune, M. Grunze, A. Straub and F. Jung, *Biointerphases*, 2013, **8**, 33.
31 M. Hedayati, M. J. Neufeld, M. M. Reynolds and M. J. Kipper, *Mater. Sci. Eng., R*, 2019, **138**, 118–152.

32 R. Puri, V. Auffret and J. Rodes-Cabau, *J. Am. Coll. Cardiol.*, 2017, **69**, 2193–2211.
33 V. J. Nijenhuis, J. Brouwer, R. Delewi, R. S. Hermanides, W. Holvoet, C. L. F. Dubois, P. Frambach, B. De Bruyne, G. K. van Houwelingen, J. A. S. Van Der Heyden, P. Tousek, F. van der Kley, I. Buysschaert, C. E. Schotborgh, B. Ferdinande, P. van der Harst, J. Roosen, J. Peper, F. W. F. Thielen, L. Veenstra, D. R. P. P. Chan Pin Yin, M. J. Swaans, B. Rensing, A. W. J. van 't Hof, L. Timmers, J. C. Kelder, P. R. Stella, J. Baan and J. M. ten Berg, *N. Engl. J. Med.*, 2020, **382**, 1696–1707.
34 A. J. Ullman, A. C. Bulmer, T. R. Dargaville, C. M. Rickard and V. Chopra, *Expert Rev. Med. Devices*, 2019, **16**, 25–33.
35 I. Reviakine, F. Jung, S. Braune, J. L. Brash, R. Latour, M. Gorbet and W. van Oeveren, *Blood Rev.*, 2017, **31**, 11–21.
36 M. Bernard, E. Jubeli, M. D. Pungente and N. Yagoubi, *Biomater. Sci.*, 2018, **6**, 2025–2053.
37 I. Sotiri, M. Robichaud, D. Lee, S. Braune, M. Gorbet, B. D. Ratner, J. L. Brash, R. A. Latour and I. Reviakine, *Acta Biomater.*, 2019, **87**, 55–60.
38 L. Reeve and P. Baldrick, *Expert Rev. Med. Devices*, 2017, **14**, 161–167.
39 U. T. Seyfert, V. Biehl and J. Schenk, *Biomol. Eng.*, 2002, **19**, 91–96.
40 W. van Oeveren, *Scientifica*, 2013, **2013**, 392584.
41 A. Podias, T. Groth and Y. Missirlis, *J. Biomater. Sci., Polym. Ed.*, 1994, **6**, 399–410.
42 H. Fu, Y. Jiang, D. Yang, F. Scheiflinger, W. P. Wong and T. A. Springer, *Nat. Commun.*, 2017, **8**, 324.
43 M. Weber, H. Steinle, S. Golombek, L. Hann, C. Schlensak, H. P. Wendel and M. Avci-Adali, *Front. Bioeng. Biotechnol.*, 2018, **6**, 99.
44 R. P. Gallegos, P. J. Nockel, A. L. Rivard and R. W. Bianco, *J. Heart Valve Dis.*, 2005, **14**, 423–432.
45 B. L. Zhang, R. W. Bianco and F. J. Schoen, *Front. Cardiovasc. Med.*, 2019, **6**, 72.
46 H. Du, C. Li, Y. F. Luan, Q. Liu, W. K. Yang, Q. Yu, D. Li, J. L. Brash and H. Chen, *Mater. Horiz.*, 2016, **3**, 556–562.
47 V. Jokinen, E. Kankuri, S. Hoshian, S. Franssila and R. H. A. Ras, *Adv. Mater.*, 2018, **30**, e1705104.
48 B. D. Ippel and P. Y. W. Dankers, *Adv. Healthcare Mater.*, 2018, **7**, 1700505.
49 S. Peppou-Chapman, J. K. Hong, A. Waterhouse and C. Neto, *Chem. Soc. Rev.*, 2020, **49**, 3688–3715.
50 G. Mackie, L. Gao, S. Yau, D. C. Leslie and A. Waterhouse, *Trends Biotechnol.*, 2019, **37**, 268–280.
51 C. Howell, A. Grinthal, S. Sunny, M. Aizenberg and J. Aizenberg, *Adv. Mater.*, 2018, **30**, e1802724.
52 K. S. Lavery, C. Rhodes, A. McGraw and M. J. Eppihimer, *Adv. Drug Delivery Rev.*, 2017, **112**, 2–11.
53 X. Liu, L. Yuan, D. Li, Z. Tang, Y. Wang, G. Chen, H. Chen and J. L. Brash, *J. Mater. Chem. B*, 2014, **2**, 5718–5738.
54 H. H. Lipowsky, *Microcirculation*, 2005, **12**, 5–15.
55 A. Marossy, P. Svorc, I. Kron and S. Gresova, *Clin. Hemorheol. Microcirc.*, 2009, **42**, 239–258.
56 R. J. Hunter, *Foundations of Colloid Science*, Oxford University Press, Oxford, 1993.
57 D. F. Evans and H. Wennerstrom, *The Colloidal Domain*, Wiley-VCH, New York, 1999.
58 B. J. Ballermann, A. Dardik, E. Eng and A. Liu, *Kidney Int. Suppl.*, 1998, **67**, S100–S108.
59 D. Katritsis, L. Kaiktsis, A. Chaniotis, J. Pantos, E. P. Efstathopoulos and V. Marmarelis, *Prog. Cardiovasc. Dis.*, 2007, **49**, 307–329.
60 L. F. Brass and S. L. Diamond, *J. Thromb. Haemostasis*, 2016, **14**, 906–917.
61 F. M. White, *Fluid Mechanics*, McGraw Hill, 2011.
62 G. A. Pop, D. J. Duncker, M. Gardien, P. Vranckx, S. Versluis, D. Hasan and C. J. Slager, *Neth. Heart J.*, 2002, **10**, 512–516.
63 R. E. Wells, Jr., R. Denton and E. W. Merrill, *J. Lab. Clin. Med.*, 1961, **57**, 646–656.
64 M. M. Alves, C. Rocha and M. P. Goncalves, *Clin. Hemorheol. Microcirc.*, 2013, **53**, 369–386.
65 R. E. Wells, Jr. and E. W. Merrill, *Science*, 1961, **133**, 763–764.
66 J. T. Brundage, *Am. J. Physiol.*, 1934, **110**, 659–665.
67 W. S. Nesbitt, E. Westein, F. J. Tovar-Lopez, E. Tolouei, A. Mitchell, J. Fu, J. Carberry, A. Fouras and S. P. Jackson, *Nat. Med.*, 2009, **15**, 665–673.
68 Y. Qiu, D. R. Myers and W. A. Lam, *Nat. Rev. Mater.*, 2019, **4**, 294–311.
69 R. Piper, P. J. Carr, L. J. Kelsey, A. C. Bulmer, S. Keogh and B. J. Doyle, *Sci. Rep.*, 2018, **8**, 3441.
70 K. Bourque, C. Cotter, C. Dague, D. Harjes, O. Dur, J. Duhamel, K. Spink, K. Walsh and E. Burke, *ASAIO J.*, 2016, **62**, 375–383.
71 K. H. Fraser, M. E. Taskin, B. P. Griffith and Z. J. Wu, *Med. Eng. Phys.*, 2011, **33**, 263–280.
72 I. Birschmann, M. Dittrich, T. Eller, B. Wiegmann, A. J. Reininger, U. Budde and M. Struber, *J. Heart Lung Transplant.*, 2014, **33**, 80–87.
73 N. Moazami, K. Fukamachi, M. Kobayashi, N. G. Smedira, K. J. Hoercher, A. Massiello, S. Lee, D. J. Horvath and R. C. Starling, *J. Heart Lung Transplant.*, 2013, **32**, 1–11.
74 J. Charonko, S. Karri, J. Schmieg, S. Prabhu and P. Vlachos, *Ann. Biomed. Eng.*, 2009, **37**, 1310–1321.
75 Y. Cadroy, T. A. Horbett and S. R. Hanson, *J. Lab. Clin. Med.*, 1989, **113**, 436–448.
76 M. Koupenova, B. E. Kehrel, H. A. Corkrey and J. E. Freedman, *Eur. Heart J.*, 2017, **38**, 785–791.
77 R. P. McEver and C. Zhu, *Annu. Rev. Cell. Dev. Biol.*, 2010, **26**, 363–396.
78 J. W. Weisel and R. I. Litvinov, *J. Thromb. Haemostasis*, 2019, **17**, 271–282.
79 A. Bonnefoy, Q. D. Liu, C. Legrand and M. M. Frojmovic, *Biophys. J.*, 2000, **78**, 2834–2843.
80 T. P. Nifong and T. J. McDevitt, *Chest*, 2011, **140**, 48–53.

81 T. K. Liem, K. E. Yanit, S. E. Moseley, G. J. Landry, T. G. Deloughery, C. A. Rumwell, E. L. Mitchell and G. L. Moneta, *J. Vasc. Surg.*, 2012, **55**, 761–767.
82 R. S. Evans, J. H. Sharp, L. H. Linford, J. F. Lloyd, S. C. Woller, S. M. Stevens, C. G. Elliott, J. S. Tripp, S. S. Jones and L. K. Weaver, *Chest*, 2013, **143**, 627–633.
83 M. H. Kroll, J. D. Hellums, L. V. McIntire, A. I. Schafer and J. L. Moake, *Blood*, 1996, **88**, 1525–1541.
84 L. D. Casa, D. H. Deaton and D. N. Ku, *J. Vasc. Surg.*, 2015, **61**, 1068–1080.
85 J. R. O'Brien, *Lancet*, 1990, **335**, 711–713.
86 B. Sebastian and P. S. Dittrich, *Annu. Rev. Fluid Mech.*, 2018, **50**, 483–504.
87 C. A. Siedlecki, B. J. Lestini, K. K. Kottke-Marchant, S. J. Eppell, D. L. Wilson and R. E. Marchant, *Blood*, 1996, **88**, 2939–2950.
88 S. W. Schneider, S. Nuschele, A. Wixforth, C. Gorzelanny, A. Alexander-Katz, R. R. Netz and M. F. Schneider, *Proc. Natl. Acad. Sci. U. S. A.*, 2007, **104**, 7899–7903.
89 M. V. Kameneva, G. W. Burgreen, K. Kono, B. Repko, J. F. Antaki and M. Umezu, *ASAIO J.*, 2004, **50**, 418–423.
90 S. E. Olia, T. M. Maul, J. F. Antaki and M. V. Kameneva, *Int. J. Artif. Organs*, 2016, **39**, 150–159.
91 C. C. Helms, M. Marvel, W. Zhao, M. Stahle, R. Vest, G. J. Kato, J. S. Lee, G. Christ, M. T. Gladwin, R. R. Hantgan and D. B. Kim-Shapiro, *J. Thromb. Haemostasis*, 2013, **11**, 2148–2154.
92 P. C. Minneci, K. J. Deans, H. Zhi, P. S. Yuen, R. A. Star, S. M. Banks, A. N. Schechter, C. Natanson, M. T. Gladwin and S. B. Solomon, *J. Clin. Invest.*, 2005, **115**, 3409–3417.
93 J. T. Horobin, S. Sabapathy and M. J. Simmonds, *Artif. Organs*, 2017, **41**, 1017–1025.
94 C. Meierhofer, E. P. Schneider, C. Lyko, A. Hutter, S. Martinoff, M. Markl, A. Hager, J. Hess, H. Stern and S. Fratz, *Eur. Heart J. Cardiovasc. Imaging*, 2013, **14**, 797–804.
95 P. van Ooij, M. Markl, J. D. Collins, J. C. Carr, C. Rigsby, R. O. Bonow, S. C. Malaisrie, P. M. McCarthy, P. W. M. Fedak and A. J. Barker, *J Am Heart Assoc*, 2017, **6**, e005959.
96 E. Bollache, P. W. M. Fedak, P. van Ooij, O. Rahman, S. C. Malaisrie, P. M. McCarthy, J. C. Carr, A. Powell, J. D. Collins, M. Markl and A. J. Barker, *J. Thorac. Cardiovasc. Surg.*, 2018, **155**, 2277–2286.
97 C. H. Yap, N. Saikrishnan and A. P. Yoganathan, *Biomech. Model. Mechanobiol.*, 2012, **11**, 231–244.
98 R. Torii, I. El-Hamamsy, M. Donya, S. V. Babu-Narayan, M. Ibrahim, P. J. Kilner, R. H. Mohiaddin, X. Y. Xu and M. H. Yacoub, *J. Thorac. Cardiovasc. Surg.*, 2012, **143**, 1422–1428.
99 A. Nascimbene, S. Neelamegham, O. H. Frazier, J. L. Moake and J. F. Dong, *Blood*, 2016, **127**, 3133–3141.
100 C. K. Holland, J. M. Brown, L. M. Scoutt and K. J. Taylor, *Ultrasound Med. Biol.*, 1998, **24**, 1079–1086.
101 J. J. Wentzel, Y. S. Chatzizisis, F. J. Gijsen, G. D. Giannoglou, C. L. Feldman and P. H. Stone, *Cardiovasc. Res.*, 2012, **96**, 234–243.
102 E. S. Weydahl and J. E. Moore, *J. Biomech.*, 2001, **34**, 1189–1196.
103 H. Zafar, F. Sharif and M. J. Leahy, *Int. J. Cardiol. Heart Vasc.*, 2014, **5**, 68–71.
104 C. P. Cheng, R. J. Herfkens and C. A. Taylor, *Am. J. Physiol.: Heart Circ. Physiol.*, 2003, **284**, H1161–H1167.
105 G. Ciuti, D. Righi, L. Forzoni, A. Fabbri and A. M. Pignone, *Am. J. Neuroradiol.*, 2013, **34**, 2000–2004.
106 S. P. Jackson, *Blood*, 2007, **109**, 5087–5095.
107 B. P. Selgrade and G. A. Truskey, *Artif. Organs*, 2012, **36**, E89–E96.
108 S. Gross-Hardt, F. Hesselmann, J. Arens, U. Steinseifer, L. Vercaemst, W. Windisch, D. Brodie and C. Karagiannidis, *Crit. Care*, 2019, **23**, 348.
109 D. McPherson, O. Adekanye, A. R. Wilkes and J. E. Hall, *Anesth. Analg.*, 2009, **108**, 1198–1202.
110 F. Rikhtegar, F. Pacheco, C. Wyss, K. S. Stok, H. Ge, R. J. Choo, A. Ferrari, D. Poulikakos, R. Muller and V. Kurtcuoglu, *PLoS One*, 2013, **8**, e58147.
111 M. Sanmartin, J. Goicolea, C. Garcia, J. Garcia, A. Crespo, J. Rodriguez and J. M. Goicolea, *Rev. Esp. Cardiol.*, 2006, **59**, 20–27.
112 J. J. Wentzel, D. M. Whelan, W. J. van der Giessen, H. M. M. van Beusekom, I. Andhyiswara, P. W. Serruys, C. J. Slager and R. Krams, *J. Biomech.*, 2000, **33**, 1287–1295.
113 M. I. Papafaklis, C. V. Bourantas, P. E. Theodorakis, C. S. Katsouras, K. K. Naka, D. I. Fotiadis and L. K. Michalis, *JACC Cardiovasc Interv*, 2010, **3**, 1181–1189.
114 V. Raghav, I. Okafor, M. Quach, L. Dang, S. Marquez and A. P. Yoganathan, *Ann. Thorac. Surg.*, 2016, **101**, 1759–1765.
115 F. Khalili, P. P. T. Gamage and H. A. Mansy, *J. Appl. Biotechnol. Bioeng.*, 2017, **2**, 187–191.
116 H. A. Dwyer, P. B. Matthews, A. Azadani, L. Ge, T. S. Guy and E. E. Tseng, *J. Thorac. Cardiovasc. Surg.*, 2009, **138**, 1227–1233.
117 D. Hasler and D. Obrist, *PLoS One*, 2018, **13**, e0194384.
118 Q. Li, F. Hegner and C. H. Bruecker, *J. Biomech. Eng.*, 2020, **142**, 011006.
119 S. Baratchi, M. T. K. Zaldivia, M. Wallert, J. Loseff-Silver, S. Al-Aryahi, J. Zamani, P. Thurgood, A. Salim, N. M. Htun, D. Stub, P. Vahidi, S. J. Duffy, A. Walton, T. H. Nguyen, A. Jaworowski, K. Khoshmanesh and K. Peter, *Circulation*, 2020, **142**, 1092–1105.
120 J. J. Hathcock, *Arterioscler., Thromb., Vasc. Biol.*, 2006, **26**, 1729–1737.
121 D. H. Lee and J. M. de la Torre Hernandez, *Eur. Cardiol.*, 2018, **13**, 54–59.
122 S. J. Wilson, D. E. Newby, D. Dawson, J. Irving and C. Berry, *Heart*, 2017, **103**, 573–580.
123 M. Alkhouli, A. Farooq, R. S. Go, S. Balla and C. Berzingi, *Clin. Cardiol.*, 2019, **42**, 692–700.
124 H. D. Polaschegg, *Semin. Dial.*, 2009, **22**, 524–531.

125 S. S. Abbas, M. S. Nasif, R. Al-Waked and M. A. Meor Said, *Artif. Organs*, 2020, **44**, E20–E39.
126 G. Fuchs, N. Berg, L. M. Broman and L. Prahl Wittberg, *Sci. Rep.*, 2018, **8**, 13985.
127 M. B. Farag, C. Karmonik, F. Rengier, M. Loebe, M. Karck, H. von Tengg-Kobligk, A. Ruhparwar and S. Partovi, *Methodist Debakey Cardiovasc. J.*, 2014, **10**, 185–189.
128 S. S. Najjar, M. S. Slaughter, F. D. Pagani, R. C. Starling, E. C. McGee, P. Eckman, A. J. Tatooles, N. Moazami, R. L. Kormos, D. R. Hathaway, K. B. Najarian, G. Bhat, K. D. Aaronson, S. W. Boyce and H. B. t. T. A. T. Investigators, *J. Heart Lung Transplant.*, 2014, **33**, 23–34.
129 K. Bourque, C. Cotter, C. Dague, D. Harjes, O. Dur, J. Duhamel, K. Spink, K. Walsh and E. Burke, *ASAIO J.*, 2016, **62**, 375–383.
130 A. R. Curtas, H. G. Wood, P. E. Allaire, J. C. McDaniel, S. W. Day and D. B. Olsen, *ASAIO J.*, 2002, **48**, 552–561.
131 Y. Zhang, B. Gao and C. Yu, *Comput. Methods Programs Biomed.*, 2016, **133**, 217–227.
132 M. Huang, S. Fan, W. Xing and C. Liu, *Math. Comput. Model.*, 2010, **52**, 2036–2042.
133 J. Linneweber, P. M. Dohmen, U. Kertzscher, K. Affeld, Y. Nose and W. Konertz, *Artif. Organs*, 2007, **31**, 345–351.
134 W. van Oeveren, I. F. Tielliu and J. de Hart, *Int. J. Biomater.*, 2012, **2012**, 673163.
135 K. R. Forrester, C. Stewart, J. Tulip, C. Leonard and R. C. Bray, *Med. Biol. Eng. Comput.*, 2002, **40**, 687–697.
136 J. Shang, Z. Chen, M. Wang, Q. Li, W. Feng, Y. Wu, W. Wu, M. P. Graziano and M. Chintala, *Thromb. Res.*, 2014, **134**, 433–439.
137 D. M. Mizurini, I. M. Francischetti, J. F. Andersen and R. Q. Monteiro, *Thromb. Haemostasis*, 2010, **104**, 1116–1123.
138 A. K. Dunn, H. Bolay, M. A. Moskowitz and D. A. Boas, *J. Cereb. Blood Flow Metab.*, 2001, **21**, 195–201.
139 M. Linden, H. Golster, S. Bertuglia, A. Colantuoni, F. Sjoberg and G. Nilsson, *Microvasc. Res.*, 1998, **56**, 261–270.
140 R. J. Roman and C. Smits, *Am. J. Physiol.*, 1986, **251**, F115–F124.
141 G. Smedley, K. P. Yip, A. Wagner, S. Dubovitsky and D. J. Marsh, *IEEE Trans. Biomed. Eng.*, 1993, **40**, 290–297.
142 S. W. Jordan, C. A. Haller, R. E. Sallach, R. P. Apkarian, S. R. Hanson and E. L. Chaikof, *Biomaterials*, 2007, **28**, 1191–1197.
143 L. G. Durand, D. Garcia, F. Sakr, H. Sava, R. Cimon, P. Pibarot, A. Fenster and J. G. Dumesnil, *J. Heart Valve Dis.*, 1999, **8**, 85–95.
144 G. E. Engels, S. L. Blok and W. van Oeveren, *Biointerphases*, 2016, **11**, 031004.
145 C. L. Haycox and B. D. Ratner, *J. Biomed. Mater. Res.*, 1993, **27**, 1181–1193.
146 J. Brubert, S. Krajewski, H. P. Wendel, S. Nair, J. Stasiak and G. D. Moggridge, *J. Mater. Sci.: Mater. Med.*, 2016, **27**, 32.
147 H. Touma, I. Sahin, T. Gaamangwe, M. B. Gorbet and S. D. Peterson, *J. Biomech. Eng.*, 2014, **136**, 071004.
148 S. M. Hastings, M. T. Griffin and D. N. Ku, *Platelets*, 2017, **28**, 427–433.
149 S. Jahanmir, A. Z. Hunsberger, H. Heshmat, M. J. Tomaszewski, J. F. Walton, W. J. Weiss, B. Lukic, W. E. Pae, C. M. Zapanta and T. Z. Khalapyan, *Artif. Organs*, 2008, **32**, 366–375.
150 A. Redaelli, F. Boschetti and F. Inzoli, *Comput. Biol. Med.*, 1997, **27**, 233–247.
151 M. G. Al-Azawy, A. Turan and A. Revell, *Comput. Methods Biomech. Biomed. Eng.*, 2016, **19**, 271–285.
152 D. N. Sarode and S. Roy, *Expert Rev. Med. Devices*, 2019, **16**, 603–616.
153 R. A. Gardner, *J. Lab. Clin. Med.*, 1974, **84**, 494–508.
154 R. Y. Kannan, H. J. Salacinski, J. De Groot, I. Clatworthy, L. Bozec, M. Horton, P. E. Butler and A. M. Seifalian, *Biomacromolecules*, 2006, **7**, 215–223.
155 S. A. Mousa, S. Khurana and M. S. Forsythe, *Arterioscler., Thromb., Vasc. Biol.*, 2000, **20**, 1162–1167.
156 M. Othman and H. Kaur, in *Hemostasis and Thrombosis: Methods and Protocols*, ed. E. J. Favaloro and G. Lippi, Springer New York, New York, NY, 2017, pp. 533–543, DOI: 10.1007/978-1-4939-7196-1_39.
157 M. Pressly, M. D. Neal, G. Clermont and R. S. Parker, presented in part at the Foundations of Computer Aided Process Operations/Chemical Process Control, Tuscan, AZ, 2016.
158 M. Ranucci, T. Laddomada, M. Ranucci and E. Baryshnikova, *Physiol. Rep.*, 2014, **2**, e12065.
159 M. Ranucci, M. Ranucci and E. Baryshnikova, *Blood Coagulation Fibrinolysis*, 2018, **29**, 172–177.
160 T. R. Roberts, D. C. Leslie, A. P. Cap, L. C. Cancio and A. I. Batchinsky, *J. Biomed. Mater. Res., Part B*, 2020, **108**, 496–502.
161 D. Whiting and J. A. DiNardo, *Am. J. Hematol.*, 2014, **89**, 228–232.
162 H. Shankaran and S. Neelamegham, *Biorheology*, 2001, **38**, 275–304.
163 V. Balasubramanian and S. M. Slack, *J. Biomater. Sci., Polym. Ed.*, 2002, **13**, 543–561.
164 M. A. Jamiolkowski, D. D. Pedersen, W. T. Wu, J. F. Antaki and W. R. Wagner, *Biomaterials*, 2016, **96**, 72–83.
165 M. A. Jamiolkowski, J. R. Woolley, M. V. Kameneva, J. F. Antaki and W. R. Wagner, *J. Biomed. Mater. Res., Part A*, 2015, **103**, 1303–1311.
166 T. Kragh, J. Schaller, U. Kertzscher, K. Affeld, A. Reininger and M. Spannagl, *Microfluid. Nanofluid.*, 2015, **19**, 155–167.
167 L. Krishnan, N. Varghese, C. Muraleedharan, G. Bhuvaneshwar, F. Derangere, Y. Sampeur and R. Suryanarayanan, *Biomol. Eng.*, 2002, **19**, 251–253.

168 L. M. Liu, Y. Koo, B. Collins, Z. G. Xu, J. Sankar and Y. Yun, *PLoS One*, 2017, **12**, e0182914.
169 R. D. Schaub, M. V. Kameneva, H. S. Borovetz and W. R. Wagner, *J. Biomed. Mater. Res.*, 2000, **49**, 460–468.
170 Y. Wu, M. Zhang, K. D. Hauch and T. A. Horbett, *J. Biomed. Mater. Res., Part A*, 2008, **85**, 829–839.
171 A. de Mel, K. Chaloupka, Y. Malam, A. Darbyshire, B. Cousins and A. M. Seifalian, *J. Biomed. Mater. Res., Part A*, 2012, **100**, 2348–2357.
172 B. Korpallova, M. Samos, T. Bolek, I. Skornova, F. Kovar, P. Kubisz, J. Stasko and M. Mokan, *Clin. Appl. Thromb./Hemostasis*, 2018, **24**, 1199–1207.
173 F. Skovborg, A. V. Nielsen and J. Schlichtkrull, *Scand. J. Clin. Lab. Invest.*, 1968, **21**, 83–88.
174 C. J. Glover, L. V. McIntire, L. B. Leverett, J. D. Hellums, C. H. Brown and E. A. Natelson, *Trans. - Am. Soc. Artif. Intern. Organs*, 1974, **20B**, 463–468.
175 I. V. Shevchuk, *J. Heat Transfer-Trans. ASME*, 2011, **133**, 024502.
176 G. Girdhar and D. Bluestein, *Expert Rev. Med. Devices*, 2008, **5**, 167–181.
177 R. Tran, D. R. Myers, J. Ciciliano, E. L. Trybus Hardy, Y. Sakurai, B. Ahn, Y. Qiu, R. G. Mannino, M. E. Fay and W. A. Lam, *J. Cell. Mol. Med.*, 2013, **17**, 579–596.
178 J. N. Topper, J. Cai, Y. Qiu, K. R. Anderson, Y. Y. Xu, J. D. Deeds, R. Feeley, C. J. Gimeno, E. A. Woolf, O. Tayber, G. G. Mays, B. A. Sampson, F. J. Schoen, M. A. Gimbrone, Jr. and D. Falb, *Proc. Natl. Acad. Sci. U. S. A.*, 1997, **94**, 9314–9319.
179 N. Watanabe, T. Shimada, M. Hakozaki and R. Hara, *Int. J. Artif. Organs*, 2018, **41**, 838–844.
180 A. L. Samson, I. Alwis, J. A. A. Maclean, P. Priyananda, B. Hawkett, S. M. Schoenwaelder and S. P. Jackson, *Blood*, 2017, **130**, 2453–2462.
181 V. Tutwiler, H. Wang, R. I. Litvinov, J. W. Weisel and V. B. Shenoy, *Biophys. J.*, 2017, **112**, 714–723.
182 I. V. Shevchuk, *J. Heat Transfer*, 2011, **133**, 024502.
183 K. Bataineh, *J. Fluids Eng.-Trans. ASME*, 2014, **136**, 101201.
184 K. M. Bataineh, *Comput. Fluids*, 2014, **101**, 105–113.
185 M. Sanak, B. Jakiela and W. Wegrzyn, *Bull. Pol. Acad. Sci.: Tech. Sci.*, 2010, **58**, 317–322.
186 B. Shenkman, N. Savion, R. Dardik, I. Tamarin and D. Varon, *Thromb. Res.*, 2000, **99**, 353–361.
187 J. M. Lackner, W. Waldhauser, P. Hartmann, F. Bruckert, M. Weidenhaupt, R. Major, M. Sanak, M. Wiesinger and D. Heim, *J. Funct. Biomater.*, 2012, **3**, 283–297.
188 N. P. Rhodes, A. P. Shortland, A. Rattray and D. F. Williams, *J. Mater. Sci. Mater. Med.*, 1998, **9**, 767–772.
189 T. M. Alkhamis, R. L. Beissinger and J. R. Chediak, *Blood*, 1990, **75**, 1568–1575.
190 T. M. Alkhamis, R. L. Beissinger and J. R. Chediak, *Biomaterials*, 1993, **14**, 865–870.
191 T. B. Tschopp and H. R. Baumgartner, *Thromb. Haemostasis*, 1976, **35**, 334–341.
192 A. Mzyk, G. Imbir, K. Trembecka-Wojciga, J. M. Lackner, H. Plutecka, E. Jasek-Gajda, J. Kawalko and R. Major, *ACS Biomater. Sci. Eng.*, 2020, **6**, 898–911.
193 J. J. Chiu and S. Chien, *Physiol. Rev.*, 2011, **91**, 327–387.
194 C. Sperling, M. F. Maitz and C. Werner, in *Hemocompatibility of Biomaterials for Clinical Applications*, 2018, pp. 77–104, DOI: 10.1016/b978-0-08-100497-5.00005-7.
195 A. J. Davies, *Meas. Sci. Technol.*, 2015, **26**, 127001.
196 L. H. O. Hellström, M. A. Samaha, K. M. Wang, A. J. Smits and M. Hultmark, *Meas. Sci. Technol.*, 2015, **26**, 015301.
197 R. Cardinaels, N. K. Reddy and C. Clasen, *Rheol. Acta*, 2019, **58**, 525–538.
198 R. Van Kruchten, J. M. Cosemans and J. W. Heemskerk, *Platelets*, 2012, **23**, 229–242.
199 M. Zhang, Y. Wu, K. Hauch and T. A. Horbett, *J. Biomater. Sci., Polym. Ed.*, 2008, **19**, 1383–1410.
200 T. V. Colace and S. L. Diamond, *Arterioscler. Thromb. Vasc. Biol.*, 2013, **33**, 105–113.
201 H. Lee, W. Na, B. K. Lee, C. S. Lim and S. Shin, *Clin. Hemorheol. Microcirc.*, 2019, **71**, 249–266.
202 A. Burklund, A. Tadimety, Y. Nie, N. Hao and J. X. Zhang, in *Adv. Clin. Chem*, Elsevier, 2020, vol. 95, pp. 1–72.
203 A. Brown, G. Burke and B. J. Meenan, *Biotechnol. Bioeng.*, 2011, **108**, 1148–1158.
204 F. J. Tovar-Lopez, G. Rosengarten, E. Westein, K. Khoshmanesh, S. P. Jackson, A. Mitchell and W. S. Nesbitt, *Lab Chip*, 2010, **10**, 291–302.
205 N. J. Kent, L. Basabe-Desmonts, G. Meade, B. D. MacCraith, B. G. Corcoran, D. Kenny and A. J. Ricco, *Biomed. Microdevices*, 2010, **12**, 987–1000.
206 J. M. Koo and C. Kleinstreuer, *J. Micromech. Microeng.*, 2003, **13**, 568–579.
207 R. G. Bacabac, T. H. Smit, S. C. Cowin, J. J. Van Loon, F. T. Nieuwstadt, R. Heethaar and J. Klein-Nulend, *J. Biomech.*, 2005, **38**, 159–167.
208 N. Kawagoishi, C. Nojiri, K. Senshu, T. Kido, H. Nagai, T. Kanamori, K. Sakai, H. Koyanagi and T. Akutsu, *Artif. Organs*, 1994, **18**, 588–595.
209 Y. Wu, M. Zhang, K. D. Hauch and T. A. Horbett, *J. Biomed. Mater. Res., Part A*, 2008, **85**, 829–839.
210 M. Zhang and T. A. Horbett, *J. Biomed. Mater. Res., Part A*, 2009, **89**, 791–803.
211 D. C. Leslie, A. Waterhouse, J. B. Berthet, T. M. Valentin, A. L. Watters, A. Jain, P. Kim, B. D. Hatton, A. Nedder, K. Donovan, E. H. Super, C. Howell, C. P. Johnson, T. L. Vu, D. E. Bolgen, S. Rifai, A. R. Hansen, M. Aizenberg, M. Super, J. Aizenberg and D. E. Ingber, *Nat. Biotechnol.*, 2014, **32**, 1134–1140.
212 L. Waite, *Applied biofluid mechanics*, McGraw-Hill, New York, 2007.
213 K. Vahidkhah, S. L. Diamond and P. Bagchi, *Biophys. J.*, 2014, **106**, 2529–2540.
214 L. D. Casa and D. N. Ku, *Biomed. Microdevices*, 2014, **16**, 115–126.

215 D. P. Sarvepalli, D. W. Schmidtke and M. U. Nollert, *Ann. Biomed. Eng.*, 2009, **37**, 1331–1341.
216 R. G. Mannino, D. R. Myers, B. Ahn, Y. Wang, R. Margo, H. Gole, A. S. Lin, R. E. Guldberg, D. P. Giddens, L. H. Timmins and W. A. Lam, *Sci. Rep.*, 2015, **5**, 12401.
217 H. Gong, B. P. Bickham, A. T. Woolley and G. P. Nordin, *Lab Chip*, 2017, **17**, 2899–2909.
218 N. P. Macdonald, J. M. Cabot, P. Smejkal, R. M. Guijt, B. Paull and M. C. Breadmore, *Anal. Chem.*, 2017, **89**, 3858–3866.
219 P. F. Costa, H. J. Albers, J. E. A. Linssen, H. H. T. Middelkamp, L. van der Hout, R. Passier, A. van den Berg, J. Malda and A. D. van der Meer, *Lab Chip*, 2017, **17**, 2785–2792.
220 O. Vanderpoorten, Q. Peter, P. K. Challa, U. F. Keyser, J. Baumberg, C. F. Kaminski and T. P. J. Knowles, *Microsyst. Nanoeng.*, 2019, **5**, 40.
221 S. Waheed, J. M. Cabot, N. P. Macdonald, T. Lewis, R. M. Guijt, B. Paull and M. C. Breadmore, *Lab Chip*, 2016, **16**, 1993–2013.
222 B. W. Pearre, C. Michas, J. M. Tsang, T. J. Gardner and T. M. Otchy, *Addit. Manuf.*, 2019, **30**, 100887.
223 W.-I. Wu, K. N. Sask, J. L. Brash and P. R. Selvaganapathy, *Lab Chip*, 2012, **12**, 960–970.
224 X. Hou, Y. S. Zhang, G. T.-d. Santiago, M. M. Alvarez, J. Ribas, S. J. Jonas, P. S. Weiss, A. M. Andrews, J. Aizenberg and A. Khademhosseini, *Nat. Rev. Mater.*, 2017, **2**, 17016.
225 E. C. Filipe, M. Santos, J. Hung, B. S. L. Lee, N. Yang, A. H. P. Chan, M. K. C. Ng, J. Rnjak-Kovacina and S. G. Wise, *JACC Basic Transl. Sci.*, 2018, **3**, 38–53.
226 A. Kheradvar, E. M. Groves, L. P. Dasi, S. H. Alavi, R. Tranquillo, K. J. Grande-Allen, C. A. Simmons, B. Griffith, A. Falahatpisheh, C. J. Goergen, M. R. Mofrad, F. Baaijens, S. H. Little and S. Canic, *Ann. Biomed. Eng.*, 2015, **43**, 833–843.
227 C. J. Bettinger, K. M. Cyr, A. Matsumoto, R. Langer, J. T. Borenstein and D. L. Kaplan, *Adv. Mater.*, 2007, **19**, 2847–2850.
228 K. Ren, W. Dai, J. Zhou, J. Su and H. Wu, *Proc. Natl. Acad. Sci. U. S. A.*, 2011, **108**, 8162–8166.
229 K. AbuZineh, L. I. Joudeh, B. Al Alwan, S. M. Hamdan, J. S. Merzaban and S. Habuchi, *Sci. Adv.*, 2018, **4**, eaat5304.
230 S. B. Cheepala, A. Pitre, Y. Fukuda, K. Takenaka, Y. Zhang, Y. Wang, S. Frase, T. Pestina, T. K. Gartner, C. Jackson and J. D. Schuetz, *Blood*, 2015, **126**, 2307–2319.
231 C. S. Hansel, M. N. Holme, S. Gopal and M. M. Stevens, *Biomaterials*, 2020, **226**, 119406.
232 H. R. Manley, D. L. Potter, J. M. Heddleston, T. L. Chew, M. C. Keightley and G. J. Lieschke, *J. Leukocyte Biol.*, 2020, **108**, 455–468.
233 T. L. Liu, S. Upadhyayula, D. E. Milkie, V. Singh, K. Wang, I. A. Swinburne, K. R. Mosaliganti, Z. M. Collins, T. W. Hiscock, J. Shea, A. Q. Kohrman, T. N. Medwig, D. Dambournet, R. Forster, B. Cunniff, Y. Ruan, H. Yashiro, S. Scholpp, E. M. Meyerowitz, D. Hockemeyer, D. G. Drubin, B. L. Martin, D. Q. Matus, M. Koyama, S. G. Megason, T. Kirchhausen and E. Betzig, *Science*, 2018, **360**, eaaq1392.
234 P. Hook, T. Brito-Robinson, O. Kim, C. Narciso, H. V. Goodson, J. W. Weisel, M. S. Alber and J. J. Zartman, *Biomed. Opt. Express*, 2017, **8**, 3671–3686.
235 B. R. Blackman, K. A. Barbee and L. E. Thibault, *Ann. Biomed. Eng.*, 2000, **28**, 363–372.
236 B. R. Blackman, G. Garcia-Cardena and M. A. Gimbrone, Jr., *J. Biomech. Eng.*, 2002, **124**, 397–407.
237 N. E. Hastings, M. B. Simmers, O. G. McDonald, B. R. Wamhoff and B. R. Blackman, *Am. J. Physiol.: Cell Physiol.*, 2007, **293**, C1824–C1833.
238 J. A. Pike, V. A. Simms, C. W. Smith, N. V. Morgan, A. O. Khan, N. S. Poulter, I. B. Styles and S. G. Thomas, *Platelets*, 2020, 1–5, DOI: 10.1080/09537104.2020.1748588.
239 S. U. Siddiqui, N. K. Verma, S. Mishra and R. S. Gupta, *Appl. Math. Comput.*, 2009, **210**, 1–10.
240 J. V. Soulis, G. D. Giannoglou, Y. S. Chatzizisis, K. V. Seralidou, G. E. Parcharidis and G. E. Louridas, *Med. Eng. Phys.*, 2008, **30**, 9–19.
241 M. Ashrafizaadeh and H. Bakhshaei, *Comput. Math. Appl.*, 2009, **58**, 1045–1054.
242 G. Silva, N. Leal and V. Semiao, *Int. J. Heat Fluid Flow*, 2008, **29**, 1211–1220.
243 J. S. Raben, S. Morlacchi, F. Burzotta, F. Migliavacca and P. P. Vlachos, *J. Appl. Biomater. Funct. Mater.*, 2015, **13**, e116–e126.
244 R. A. Malinauskas, P. Hariharan, S. W. Day, L. H. Herbertson, M. Buesen, U. Steinseifer, K. I. Aycock, B. C. Good, S. Deutsch, K. B. Manning and B. A. Craven, *ASAIO J.*, 2017, **63**, 150–160.
245 R. Lima, S. Wada, S. Tanaka, M. Takeda, T. Ishikawa, K. Tsubota, Y. Imai and T. Yamaguchi, *Biomed. Microdevices*, 2008, **10**, 153–167.
246 D. Pinho, R. O. Rodrigues, V. Faustino, T. Yaginuma, J. Exposto and R. Lima, *J. Biomech.*, 2016, **49**, 2293–2298.
247 F. Ghalichi, X. Deng, A. De Champlain, Y. Douville, M. King and R. Guidoin, *Biorheology*, 1998, **35**, 281–294.
248 K. Shinohara, Y. Sugii, A. Aota, A. Hibara, M. Tokeshi, T. Kitamori and K. Okamoto, *Meas. Sci. Technol.*, 2004, **15**, 1965–1970.
249 P. Browne, A. Ramuzat, R. Saxena and A. P. Yoganathan, *Ann. Biomed. Eng.*, 2000, **28**, 39–47.
250 J. O. Taylor, B. C. Good, A. V. Paterno, P. Hariharan, S. Deutsch, R. A. Malinauskas and K. B. Manning, *Cardiovasc. Eng. Technol.*, 2016, **7**, 191–209.
251 C. Y. Schule, K. Affeld, M. Kossatz, C. O. Paschereit and U. Kertzscher, *Int. J. Artif. Organs*, 2017, **40**, 109–117.
252 U. Gülan, B. Lüthi, M. Holzner, A. Liberzon, A. Tsinober and W. Kinzelbach, *Exp. Fluids*, 2012, **53**, 1469–1485.

253 K. Takashima, R. Shimomura, T. Kitou, H. Terada, K. Yoshinaka and K. Ikeuchi, *Tribol. Int.*, 2007, **40**, 319–328.
254 N. Amor, L. Geris, J. Vander Sloten and H. Van Oosterwyck, *Acta Biomater.*, 2011, **7**, 779–790.
255 P. D. Goodman, E. T. Barlow, P. M. Crapo, S. F. Mohammad and K. A. Solen, *Ann. Biomed. Eng.*, 2005, **33**, 780–797.
256 J. S. Soares, J. Sheriff and D. Bluestein, *Biomech. Model. Mechanobiol.*, 2013, **12**, 1127–1141.
257 B. Chopard, D. R. de Sousa, J. Latt, L. Mountrakis, F. Dubois, C. Yourassowsky, P. Van Antwerpen, O. Eker, L. Vanhamme, D. Perez-Morga, G. Courbebaisse, E. Lorenz, A. G. Hoekstra and K. Z. Boudjeltia, *R. Soc. Open Sci.*, 2017, **4**, 170219.
258 H. Hosseinzadegan and D. K. Tafti, *Cardiovasc. Eng. Technol.*, 2017, **8**, 164–181.